Article

Probability Stability Evaluation of Coral Reef Limestone Reef Slopes Under Earthquake

Ruize Ma [1,2], Baifeng Ji [1,2,*], Longya Zhang [1,2], Shuang Pan [2] and Kaimeng Hu [2]

[1] Sanya Science and Education Innovation Park, Wuhan University of Technology, Sanya 572024, China; mrze@whut.edu.cn (R.M.); longyazhang@whut.edu.cn (L.Z.)

[2] School of Civil Engineering and Architecture, Wuhan University of Technology, Wuhan 430070, China; panshuang2279@163.com (S.P.); hkmeng@whut.edu.cn (K.H.)

* Correspondence: jbfeng@whut.edu.cn

Abstract: With the rapid development of island construction and the frequent occurrence of natural disasters, the stability of coral reef slopes is attracting increasing attention. This study aims to assess the dynamic stability and instability risks of coral reef slopes under different earthquake intensities. Geological data were integrated, and the Newmark method and finite element analysis were employed for probabilistic stability assessment and permanent displacement evaluation, leading to the development of a validated model for slope stability assessment. The study explored the effects of varying earthquake intensities on slope stability. Results indicate that the stratified structure significantly influences stability. Reef limestone slopes exhibited higher stability, whereas multi-layered slopes, due to looseness, were less stable. Both slope types remained stable under static conditions. Earthquake intensity substantially impacted stability, with multi-layered slopes showing instability probabilities of 48% and 100% under peak ground accelerations (PGA) of 0.3 g and 0.4 g. Under extreme seismic conditions, the permanent displacement of multi-layered coral reef slopes significantly increased. This study aims to fill the gap in previous research by incorporating the random distribution of stratigraphic parameters, conducting probabilistic stability analysis based on the random distribution of geological parameters, and thereby providing references for island reef engineering construction.

Keywords: coral reef slopes; dynamic stability; permanent displacement; probabilistic stability analysis

1. Introduction

In recent years, the rapid development of marine engineering, island infrastructure, and underground space utilization has significantly enhanced the efficiency of marine transportation and spatial utilization. These advancements highlight the importance of constructing specialized geotechnical structures in marine environments. However, as the foundation of island engineering projects, coral reef tuff and coral reef sand exhibit unique properties such as high porosity, heterogeneity, and anisotropy compared to land-based geotechnical materials [1,2]. Zhu et al. [3] noted that in depth, coral reef bodies typically exhibit a stepped, tower-like, layered structure due to development and growth patterns. The properties of coral reefs are closely related to climatic factors, such as temperature, salinity, and wave action, which have influenced the formation and mechanical behavior of reef limestone. Moreover, to reveal the staged erosional–depositional patterns of coral

reef development, Liu et al. [4] conducted a systematic analysis of multiple indicators of coral reefs at the NK-1 well of Meiji Reef, re-constructing the island's formation and evolutionary history. Coral reef bodies are frequently exposed to natural disasters such as earthquakes and tsunamis, posing significant risks of landslides and structural damage, particularly along stepped, layered slopes. These challenges underscore the complexity and risks associated with island reef engineering and demand specialized strategies to ensure the stability and safety of such projects.

As early as the 1970s, the stability assessment of coral reefs began to receive increasing attention, and this topic has been extensively analyzed and explored in recent decades. In considering the stability of coral reefs under external influences such as earthquakes and waves, significant research and discussions have been carried out. Zhang et al. [5,6] combined physical model tests with numerical simulations to investigate the stability of surrounding rock in coral reef tuff strata during tunnel excavation. Bao et al. [7,8] comprehensively incorporated three-dimensional local topography and fluid–solid interaction to establish a 3D model of Zhubi Reef. This model was employed to assess the reef's seismic response and stability, leading to the development of a viscoelastic-plastic dynamic constitutive model for coral sand material. The findings provided insights into the nonlinear seismic response of coral reef–coral sand systems in the South China Sea. Zhang et al. [9] conducted 1 g shaking table tests to analyze the seismic dynamic response of a revetment breakwater and its coral sand foundation, identifying critical response characteristics. Guo et al. [10] used the limit equilibrium and Newmark methods to simulate stresses and deformations under various seismic intensities. The analysis included the calculation of safety factors and the assessment of potential seismically induced landslides and provided valuable sliding-scale solutions. To demonstrate that geotechnical simulation methods can serve as effective tools for assessing coral reef stability, Tang et al. [11] developed a shallow coral reef profile model to evaluate reef stability under seismic and hydrodynamic conditions. The findings indicated that the stability of coral reefs is influenced by wave loads, seismic intensities, and the physical properties of reef materials. Specifically, slopes on the ocean-facing side exhibited higher stability, whereas slopes on the lagoon-facing side showed greater susceptibility to landslides under seismic and hydrodynamic impacts. Costa et al. [12] performed detailed bathymetric surveys to simulate wave propagation under varying water levels and wave conditions. Taking the complex atoll morphology into account, they investigated the effects of sea-level rise and wave refraction patterns on reef stability and geographic positioning. Wu et al. [13] applied the fast Lagrangian continuum analysis method to establish a numerical model for the coral sand-pile-superstructure system. Using hysteretic damping to describe the constitutive behavior of coral sand under cyclic stress, they explored the effects of pile diameter, relative density, and permeability of coral sand on seismic response characteristics. Wang et al. [14] employed a non-hydrostatic numerical wave solver to systematically analyze the propagation, deformation, and wave climbing processes over an artificially excavated reef. A reference for evaluating the hydrodynamic impacts of artificial pit mining on reef slopes and assessing the stability of island reef shorelines under wave action was provided.

The unique mechanical properties of coral reef tuff and coral reef sand, which distinguish them from terrestrial rocks, are critical factors that must be considered when analyzing and evaluating the stability of island reefs. Coral reef tuff, a specialized geotechnical material derived from marine organisms, is distributed across the coasts and coral reefs of regions such as Mexico, the Persian Gulf, the South China Sea, and Australia [15]. Numerous studies have been conducted to investigate the physical and mechanical properties of reef tuff, including parameters such as density, porosity, permeability, and wave velocity. For instance, Wang et al. [16] performed in situ point load tests and laboratory

uniaxial compression tests on three different cementation types of reef tuff. The research evaluated the strength indices of various reef tuffs to ensure reef foundation strength and stability. Luo et al. [17] measured physical properties such as density, porosity, and longitudinal wave velocity, revealing intrinsic correlations among these parameters. They classified reef tuff into four distinct types based on porosity and cementation mode, subsequently conducting quasi-static and dynamic compression tests. The findings showed that reef tuff compressive strength exhibited a weak correlation with strain rate, while its static tensile-to-compression ratio was slightly higher than that of terrestrial rocks. Using statistical damage theory, a dynamic damage model for reef tuff under impact loading was developed and experimentally validated. Zhang et al. [18] conducted impact tests using a split Hopkinson pressure bar (SHPB) device to analyze how growth line inclination, strain rate, and density affect the dynamic mechanical properties of reef tuff. The quantitative analysis of damage modes revealed that reef tuff exhibited a lower growth line inclination, strain rate sensitivity, and density compared to terrestrial rocks. Additionally, the stress–strain curves of reef tuff showed a prolonged elastic phase and a shortened damage phase. Wu et al. [19] explored the uniaxial compression behavior and pore structure characteristics of various reef tuff types through uniaxial compression and CT scanning tests. Xu et al. [20] investigated the effect of particle size distribution (PSD) of coral sands on the failure behavior of cemented coral sand specimens. Their study uncovered the microscopic mechanisms underlying the effects of reef tuff's physical properties on its uniaxial compression behavior and proposed a practical engineering evaluation method for reef tuff quality. The studies above provide a comprehensive analysis of coral reef stability under the influence of seismic, hydrodynamic, and excavation factors.

However, previous studies have primarily focused on the macro-level and micro-level physical–mechanical properties of reef tuffs, as well as the stability of coral reef bodies under external factors such as earthquakes and waves. The stability of coral reefs is significantly influenced by the topography of reef islands, the physical and mechanical properties of coral sand and reef tuff, and the surrounding marine hydrodynamic environment [21,22]. When considering the unique mechanical properties of coral reef tuffs, the multi-stratigraphic distribution of coral reefs, and their stability under the combined influence of seismic and hydrodynamic forces, certain complexities have not been fully addressed. Bao et al. established an effective three-dimensional seawater-island reef coupling model and conducted a dynamic seismic response analysis of the reef model. However, the model assumed an idealized stratigraphy, neglecting the multi-layered structure resulting from the cyclic depositional characteristics of reef bodies. Guo et al. [10] and Tang et al. [11] provided valuable assessments of the stability of multi-stratified coral reef slopes under seismic conditions, but they overlooked the random distribution of mechanical and physical parameters of reef limestone and coral sand. The multi-stratigraphic distribution characteristics of coral reef slopes and the random distribution of stratigraphic mechanical parameters may lead to the formation of weak zones and potential slip surfaces during seismic events, significantly impacting the stability of reef bodies and the safety of marine engineering construction [23].

The existing research literature and stratigraphic drilling data were integrated in this study, with the finite element method and boundary element method employed to establish a multi-stratigraphic numerical model of coral reefs. Various aspects, including stress distribution within the reef, permanent displacement, slope landslide risk, and probabilistic stability analysis under different seismic intensities and durations, are explored. The research results establish a seismic response analysis and probabilistic stability model for multi-stratified coral reef slopes. This model provides an effective reference for seismic response analysis in earthquake-prone regions and for the development of islands with similar structural characteristics. Additionally, it offers a theoretical foundation for the

safety assessment of above-ground engineering construction and underground space development on coral reef islands. The remainder of this paper is organized as follows: Section 2 introduces the stratigraphic parameters and model of the multi-layered slope of coral reefs. Section 3 provides an overview of the numerical simulation methods for assessing the stability of coral reef slopes under seismic loading, including stability evaluation criteria method and validation. Section 4 discusses the results of stress distribution, safety factors, instability probabilities, and permanent displacements of reef slopes under static and varying seismic intensities. Section 5 investigates the response characteristics of reef slopes under earthquakes with different peak accelerations based on stability evaluation criteria and concludes with the study's findings, significance, and limitations.

2. Computational Model

2.1. Multi-Layered Slope Structural Characteristics

Figure 1 shows the geological profile model based on the southwestern reef flat of Yongshu Reef in the Xisha Islands. The shallow coral reef body features a rock basin structure, characterized by a thick layer of reef tuff at the bottom, featuring caves and sedimentary discontinuities within the tuff. The basin edge consists of a 30–40 m-wide primary reef body. Inside the basin, loose Holocene coral reef clasts accumulate with a thickness ranging from 0 to 17 m. From the basin edge toward the center, the sediment composition transitions from strongly cemented gravel clasts to weakly cemented coarse and medium sands, and finally to unconsolidated lagoonal clasts. This indicates that the mechanical properties of the surface rock and soil layers of the reef gradually weaken from the seaward side to the lagoon side. The high strength of the reef tuff provides structural integrity, and the thick rim of the basin acts as a natural barrier, offering significant protection to buildings located within the basin. This structural configuration enhances the overall stability of the reef body [24]. Additionally, the slope on the lagoon side lacks the protective structure of the reef limestone basin, making the surface rock and soil layers on this side more vulnerable compared to the seaward side under seismic conditions. As a result, the lagoon side slope faces a higher risk of failure. Furthermore, regarding the boundary conditions of the model, we assumed that the bottom boundary of the reef model was constrained in both horizontal and vertical directions, while the left and right boundaries were constrained in the horizontal direction. The top boundary was set as a free surface.
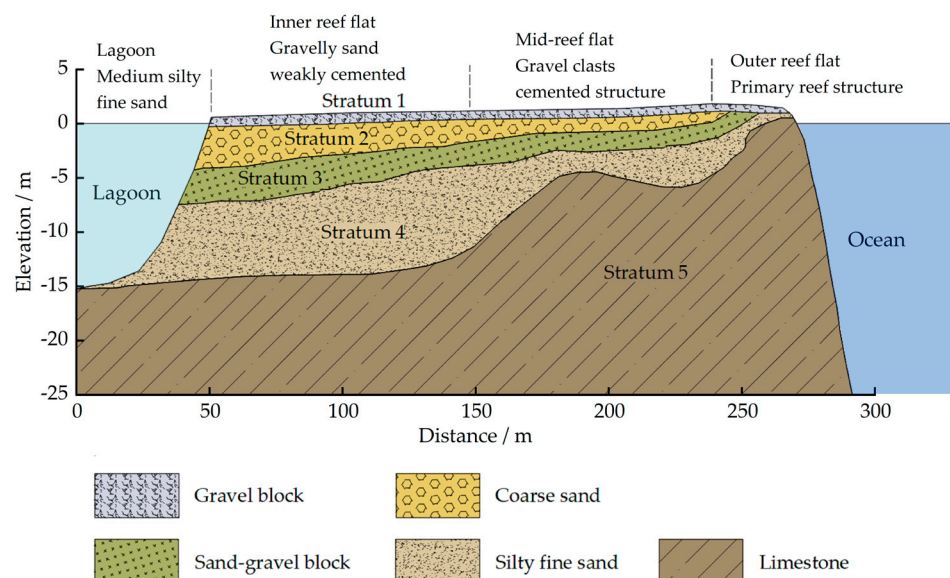
Figure 1. Geological profile diagram of the multi-stratigraphic slope of coral reef.

Significant differences exist in the structural morphology and mechanical properties between the shallow and deep reef bodies [24]. The deeper reef body consists of a reef tuff layer with high integrity and strength, forming a basin-like sedimentary foundation. In contrast, the shallow layer comprises accumulations of materials ranging from strongly cemented to unconsolidated loose sand and gravel clasts. Based on the topography and geomorphology of the coral reef body, sedimentary environment, and engineering geological characteristics, the shallow reef layer can be categorized into four structural types of reef soil bodies:

(1) Outer Reef Apron Primary Reef Structure: This structure is distributed in bands along the outer edge of the reef body. Large coral reef formations are cemented by coralline algae, creating a semi-rocky primary reef structure that can be classified as a fractured rock mass. In the southwestern part of the reef, grooves are well developed, and the slope is gentle. In contrast, other areas of the reef edge feature steeper slopes, forming rugged cliffs with minimal groove development.

(2) Middle Reef Flat Gravel Agglutination Structure: This structure is located in the raised and depressed zones of the reef flat, which represent the highest topography of the reef flat. No live coral growth is observed in this area. Large coral gravels are cemented by coralline algae swelling, with no loose sand debris accumulation. The surface layer forms a reef gravel layer, while gravel accumulations lie beneath the surface. The sediment thickness varies, becoming thinner from the outer edge of the atoll toward the interior. The underlying reef tuff exhibits a steeper gradient, while the middle layer forms a "hard layer" composed of larger breccia clasts cemented together.

(3) Inside Reef Apron Gravel-Sand Weak Cementation Structure: This structure is located within the reef apron, characterized by a surface layer of loose medium-to-coarse coral sand mixed with coral gravel blocks. The cementation is weak, and the topography is relatively flat. The burial thickness is considerable, averaging 17–18 m. Due to variations in the coral reef sedimentary facies, the vertical sedimentary layers do not exhibit a clear stratification, resulting in more homogeneous engineering geological properties.

(4) Lagoon Medium-Fine Sand Uncemented Structure: The lagoon serves as the deposition site for fine-grained coral reef detritus. Loose medium-fine sand deposits gradually thin from the edge toward the center of the lagoon, with virtually no algal cementation. The medium-fine sand accumulations exhibit good sorting and are occasionally interspersed with staghorn coral gravel blocks [25].

2.2. Stratigraphic Parameters of the Reef Limestone Model

Coral reef tuff is a unique geotechnical material of marine origin. Studies have shown that coral reef sands exhibit distinct properties compared to land-based geotechnical materials, including high porosity, heterogeneity, and anisotropy [1,3,24]. High porosity indicates the presence of numerous voids within reef limestone, significantly affecting its density characteristics. The porosity of coral reef limestone ranges from approximately 1.68% to 53%, which is notably higher than that of terrestrial rocks (typically 0–25%). The density of reef limestone varies between 1.12 and 3.07 g/cm³, whereas terrestrial rocks such as limestone and marble generally have densities ranging from 2.1 to 3 g/cm³. Reef limestone exhibits heterogeneity, meaning its composition or structure is non-uniform, as it is composed of various materials (e.g., coral fragments, shells, and sediments). Its anisotropy arises from the stratified structure formed by cyclic depositional processes [1,3]. Additionally, due to the staged erosional and depositional processes during coral reef development, the structural properties of coral reef tuff vary with depth, characterized by cyclic deposition and stratigraphic alternation [3,4]. Liu et al. [4] conducted a systematic

analysis of multiple indicators of coral reefs at the NK-1 well in Meiji Reef, reconstructing the island's formation and evolutionary history. In this study, a two-dimensional model for calculating and analyzing the stability of a shallow coral reef body was established based on previous studies and geological borehole data (shown in Figure 1). The model consists of five strata: Stratum 1: a gravel block layer composed of an unconsolidated bio-gravel sand layer; Stratum 2: a medium-to-coarse sand layer formed by loose coral bio-clastic sediments; Stratum 3: a sand and gravel block layer; Stratum 4: a silt layer consisting of Holocene loose coral detritus; Stratum 5: a framework reef tuff characterized by good lithology and stability.

The multi-layered coral reef slope geological profile model established in this study is based on geological surveys and borehole data from Yongshu Reef in the Xisha Islands, South China Sea. The model mainly relies on data from four boreholes to determine the stratigraphic characteristics. These are: (1) the Nanyong-1 borehole drilled in 1990 on the reef flat of the South China Sea, with a depth of 152.1 m, reaching the Early Pleistocene; (2) the Nanyong-2 borehole drilled in 1994, with a depth of 413.7 m, reaching the Middle Miocene of the Tertiary; (3) the Nanyong-3 borehole drilled in 1999 in the lagoon, with a depth of 5.9 m, which provides information on the sedimentary environment and paleoclimate prior to 1682; and (4) the Nanyong-4 borehole drilled in 2002, with a depth of 15.4 m, revealing earlier island reef depositional periods. These boreholes were fully investigated, including electrical logging and comprehensive analysis of the core samples [2]. Moreover, a large number of measurements and studies have been conducted on the density, porosity, permeability, wave velocity, and other related physical and mechanical properties of reef tuffs. These studies have included the analysis of coral reef body borehole data, the revelation of the stage-growth depositional mode of coral reef bodies [4], numerical simulations of coral reef body stability [7,8,10,11], static mechanical tests of reef tuff specimens [16,17], and dynamic mechanical tests [18]. The damping ratio parameters for each stratum in the coral reef slope model were sourced from the Handbook of Rock Mechanical Parameters (The Editorial Board of Manual of Engineering Geology, 2007) [10]. The shear strength parameters are primarily based on the experiments and measurements of borehole core samples conducted by Wang et al. [24]. In this study, based on data from reef tuff borehole core specimens, test results of reef tuff specimens, and stability analyses of coral reef bodies conducted by previous researchers, the distribution of material mechanical parameters for the five strata in the computational model are summarized and presented, as shown in Table 1.

Table 1. Parameters of the coral reef stratums.

Stratum	Unit Weight/kN·m⁻³	Cohesion/kPa	Angle of Internal Friction/°	Poisson's Ratio	Dumping Ratio	Shearing Modulus/MPa	Porosity	Permeability Coefficient/cm/s
1	20	20	20	0.2	0.05	72	0.3	9^{-4}
2	22	6	30	0.2	0.02	162	0.3	9^{-4}
3	22	20	30	0.17	0.08	288	0.35	9^{-4}
4	23	20	25	0.23	0.09	500	0.4	9^{-4}
5	25	1200	36	0.25	0.1	720	0.45	1^{-4}

3. Methodology

3.1. Coral Reef Slope Stability Evaluation Indicators

The evaluation of coral reef tuff slope stability primarily uses model displacement and stress as key indicators. Meanwhile, the factor of safety (FOS) is widely employed in slope stability analysis [10,11], serving as a critical measure of slope stability. The factor of safety is defined as the ratio of the slope's resistance to sliding forces to the shear stress acting on the slope. The resistance to sliding is mainly determined by the soil's cohesion, internal friction angle, and normal force, while the shear stress primarily originates from

the soil's gravity, external loads, and seismic forces. Various methods have been developed to calculate the factor of safety, including the limit equilibrium method, finite element method, and discrete element method. In this study, the Morgenstern–Price method, a widely recognized approach within the limit equilibrium method framework, was applied to evaluate the factor of safety of the coral reef tuff slope under static conditions [26].

The Morgenstern–Price method [26] is a limit equilibrium method that strictly satisfies force and moment equilibrium, making it suitable for slope stability analysis involving complex geometries and multiple stratigraphic conditions. Compared to other limit equilibrium methods (e.g., Bishop's method or Janbu's method), the Morgenstern–Price method can more accurately simulate the shape of slip surfaces and stress distribution, particularly excelling in multi-layered strata and heterogeneous materials such as reef limestone. The Morgenstern–Price method assumes that the sliding body is divided into multiple elements (soil slices), each subjected to forces such as gravity, external loads, and shear stresses. Additionally, lateral forces may develop along the sliding surface, interacting with the forces acting on the surface. For each soil slice, the method requires satisfying the equilibrium of forces along the sliding surface and in the vertical direction:

$$\Sigma F_x = 0 \, , \Sigma F_y = 0 \tag{1}$$

in the vertical direction:

$$N = W\cos\alpha - E_L\sin\alpha + E_R\sin\alpha \tag{2}$$

in the horizontal direction:

$$T = W\sin\alpha + E_L cos\alpha + E_R\sin\alpha \tag{3}$$

where N represents the normal force (kN) acting on the sliding surface; T denotes the shear stress (kPa) on the sliding surface; E_L and E_R are the lateral forces (kN) on the left and right sides of the soil slice, respectively; and α (°) is the inclination angle of the sliding surface.

The Morgenstern–Price method determines the factor of safety F through an iterative process, typically utilizing numerical methods to satisfy the equilibrium conditions for all soil slice units [26]:

$$F = \frac{\Sigma(c'b + \sigma'\tan\phi')}{\Sigma T} \tag{4}$$

where c' represents the effective cohesive force (kPa), ϕ' is the effective angle of internal friction (°), σ' denotes the normal stress (kPa), b is the width of the soil strip element (m), and T is the sliding force (kN). The iterative process ensures that both moment equilibrium and force equilibrium are satisfied simultaneously by adjusting the safety factor *F*.

For the stability analysis of island slopes under seismic loads, this paper used the Newmark Sliding Block method, a dynamic slope stability analysis technique. The Newmark method is suitable for dynamic analysis of both linear and nonlinear systems, capable of handling various types of dynamic loads and simulating the dynamic response of complex structures, including buildings, bridges, and slopes. Due to its maturity and efficiency in slope stability analysis, it is widely used in dynamic response analysis. It assumes that the slope sliding body can be simplified as a rigid block moving along the potential sliding surface. The seismic load is treated as an inertial force applied to the block due to seismic acceleration. When the horizontal component of seismic acceleration exceeds the critical acceleration k_c, the block will begin to slide along the sliding surface. The cumulative displacement during this sliding process is an important criterion for assessing slope instability or failure.

The critical acceleration is an important parameter in dynamic slope stability analysis and is related to the static factor of safety F of the slope, which is calculated as [27]:

$$k_c = g \cdot \left(\tan\phi - \frac{1}{F}\right) \tag{5}$$

where g represents the gravitational acceleration and ϕ is the friction angle (°) on the sliding surface. When the horizontal component of seismic acceleration a (t), denoted as a_h (m/s^2), exceeds the critical acceleration k_c (m/s^2), the slider begins to slide. Cumulative displacement D is also an important criterion for determining whether a slope is unstable. Table 2 presents the displacement assessment criteria for slopes. The cumulative permanent displacement evaluation standard is based on a review and summary of the studies conducted by Jibson et al. [28] and Duncan et al. [29]. The cumulative displacement D (m) is calculated by integrating over the time frames t_1 and t_2, which correspond to the periods during which sliding occurs [27,30]:

$$D = \int_{t_1}^{t_2} (a(h) - k_c) \cdot dt \tag{6}$$

Table 2. Slope instability–displacement evaluation criteria.

Cumulative Displacement	Stability Assessment	Descriptions
$D < 0.01$ m	Stable (Minimal Risk)	The slope remains essentially intact after the earthquake; no special reinforcement is required.
0.01 m $\leq D < 0.1$ m	Acceptable Stability (Minor Risk)	The slope may experience minor deformation, but overall stability is adequate.
0.1 m $\leq D < 0.5$ m	Unstable (Moderate Risk)	Significant sliding may occur; slope reinforcement should be considered.
$D \geq 0.5$ m	Failure (High Risk)	The slope exhibits substantial sliding; urgent mitigation measures are necessary.

3.2. Numerical Simulation Method for Seismic Response of Coral Island Reef Slopes

Geo-Studio [31] has been widely applied for stability analysis of geotechnical slopes under static conditions and the influence of dynamic loads, seepage, and temperature. In this study, Geo-Studio 2024.1.0 was used to perform stability assessments of reef limestone slopes under both static and dynamic conditions. Under static conditions, the stress state of the model and the slope safety factor were accurately simulated, enabling effective assessments of slope instability risk. Under dynamic conditions, the full process of seismic impacts was dynamically modeled, allowing for monitoring of stress, displacement, and instability risks in the slope model. Incorporating methods such as finite element analysis, finite difference analysis, and limit equilibrium analysis, this tool is particularly suited for solving geotechnical engineering problems such as slope stability and seismic response, with a focus on practical engineering applications compared to traditional finite element approaches. In this study, the Sigma/W module was first used to establish the initial stress field, with its core algorithm based on the finite element method. This approach divides the slope into a finite number of elements, solves the governing equations under static equilibrium, and calculates the effective stress field, total stress field, and displacement field. Subsequently, the Quake/W module was utilized to calculate the stress and displacement distribution induced by earthquakes. The Slope/W module was then employed to monitor changes in the slope's factor of safety and indicators such as permanent displacement during the seismic process, thereby evaluating the impact of earthquakes on the stability of the reef body slopes.

3.3. Method Validation

Guo et al. [10] utilized the limit equilibrium slicing method along with the Newmark method to determine the potential slip surface and slope safety factors of the Zhubi Reef slope model, a closed atoll in the Nansha Islands, under both static and dynamic conditions. The stress field distribution of the slope model and the cumulative permanent displacement were derived using the Quake/W nonlinear dynamic response analysis procedure. These results provided an effective reference for early warning of coral reef slope slippage risk and for assessing the stability of the reef body. Building on the research findings of Guo et al. [10], this study established a coral reef slope model consistent with theirs and maintained the same boundary conditions as in their study. Specifically, the bottom boundary of the model was constrained in both horizontal and vertical directions, while the left and right boundaries were constrained in the horizontal direction, with hydrostatic pressure applied to the slope boundaries on both sides. Additionally, the material parameters provided in their study were consistently input into the model. The computational results of this model are in close agreement with those of the original study, thereby validating the effectiveness of the numerical simulation method for seismic response analysis of coral reef slopes used in this research.

Figure 2a,c show the two-dimensional geological profile model of Zhubi Reef, established by Guo et al. [10], along with the model results, including the location of the critical slip surface, potential slip surface and the factor of safety for the two slopes under static conditions. Figure 2b,d illustrate a comparison between the results obtained in this study and those from prior work. Figure 3 presents a comparison between the effective stress distribution results of the reef body under static conditions obtained by Guo et al. and those from this study.
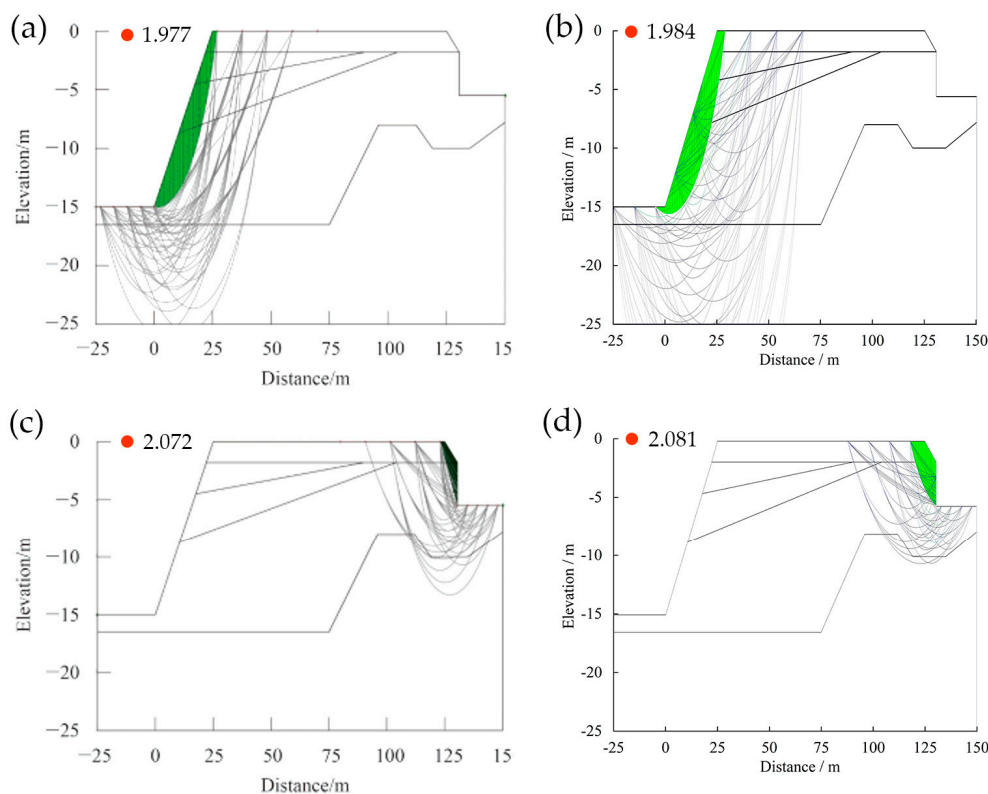
Figure 2. Comparative validation of potential slip surfaces for the 2D stratigraphic model of Zhubi Reef: (**a**,**b**) left-side slope; (**c**,**d**) right-side slope. Note: (**a**,**c**) are adapted from Guo et al. [9]. The black curve and the green area represent the potential slip surface and the critical slip surface, respectively.

Guo et al. [10] pointed out that the atoll fringing slope is a crucial part of the atoll, and its risk prediction is especially important. Using the limit equilibrium method, the potential slip surface was calculated (Figure 2), and the safety factors of the left- and right-side slope of the coral reef fringing slope under self-gravity conditions were found to be 1.977 and 2.072, respectively. It can be observed that, under self-gravity conditions, the safety factors of both side slopes of the reef were significantly higher than the destabilization threshold, indicating better slope stability. The safety factor values for the left and right slopes obtained in this study were 1.984 and 2.081, respectively, which were 0.35% and 0.43% higher than the results obtained by Guo et al. [10]. As shown in Figure 3, the effective stress distribution of the reef is relatively uniform in both the horizontal and vertical directions, further reflecting the good stability of the reef under self-gravity conditions.
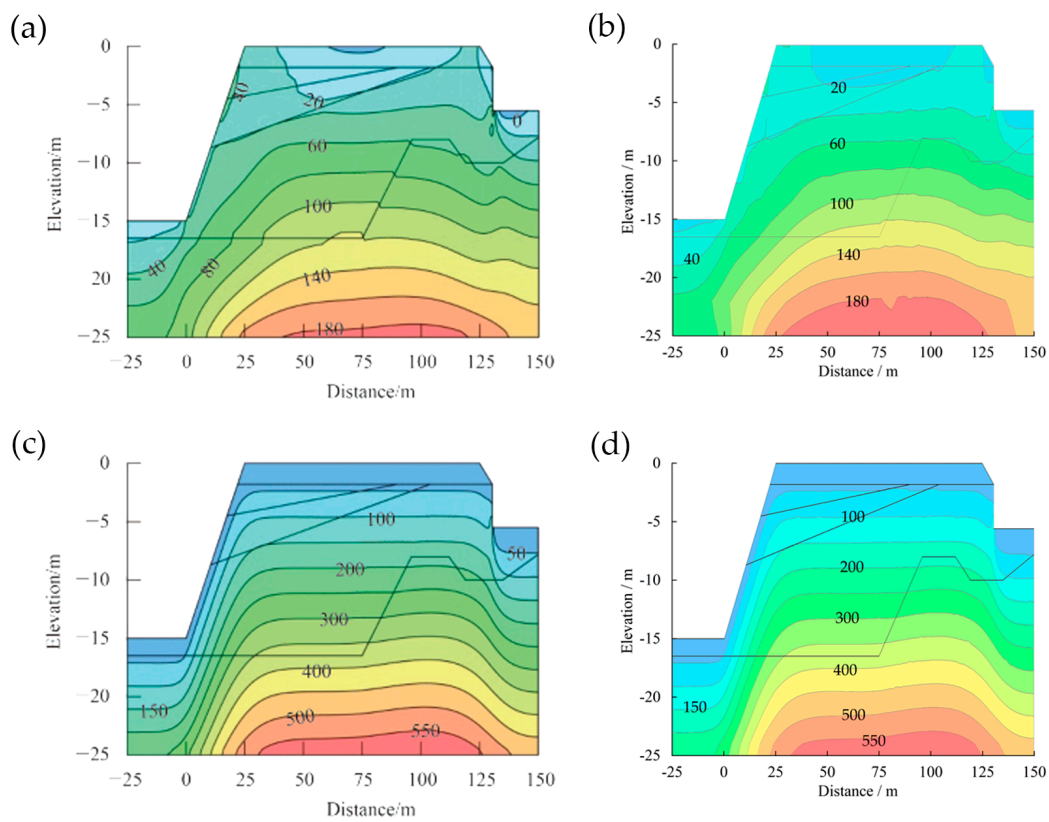
Figure 3. Comparison of the effective stress distribution results for the two-dimensional model of Zhubi Reef: (**a**,**b**) horizontal direction; (**c**,**d**) vertical direction. Note: (**a**,**c**) are adapted from Guo et al. [10].

4. Results

4.1. Static Stability of the Coral Reef Body Slopes Under Static Conditions

4.1.1. The Initial Stress Field and Slope Safety Factor

Before investigating the dynamic response behavior of coral reef bodies, it is essential to analyze their stability under natural conditions. This analysis helps to identify the risk of reef body instability, understand the internal stress state in the natural condition, and provide the initial stress field required for dynamic response analysis. The distribution of effective stress within the reef under self-gravity conditions is shown in Figure 4. The effective stress inside the reef body was relatively uniform. In the first and second strata near the reef surface, as well as the middle and inner reef apron areas, horizontal tensile stress predominated, with most values below 0.02 MPa. A small portion of the outer

middle reef apron exhibited horizontal tensile stress between 0.02 MPa and 0.04 MPa. From the third to fifth strata, horizontal effective stress increased uniformly with depth, ranging from 0 kPa to 230 kPa, while in the internal slopes on both sides of the reef, horizontal effective stress varied between 20 kPa and 180 kPa. Vertical effective stress was uniformly distributed across the reef body and increased linearly with depth, reaching a maximum of approximately 650 kPa. No tensile stress was observed on the reef's surface in the vertical direction. Additionally, effective stress on the right side of the reef was slightly higher than on the left, attributed to the gradual increase in ground level from left to right in the tuff layer of the frame reef, which had a higher unit weight.
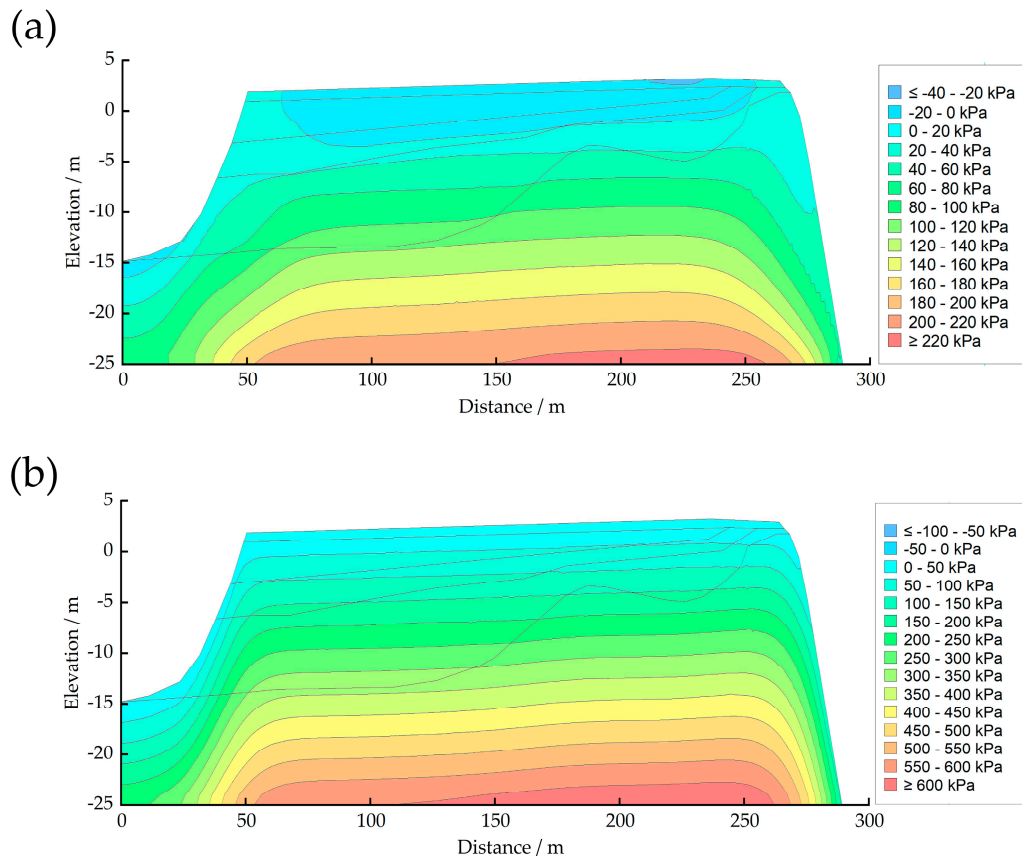
Figure 4. Distribution of effective stress in the reef body under self-weight conditions. (**a**) horizontal direction; (**b**) vertical direction.

In this study, the Morgenstern–Price method was applied to analyze the slopes on both sides of the reef under self-weight conditions (the lagoon slope on the left and the seaward slope on the right). The results, including the distribution of potential slip surfaces, critical slip surfaces, and safety factors, are shown in Figure 5. The safety factor of the left slope was 3.314, while that of the right slope was 19.026. The critical slip surface of the left slope spanned from the first to the fourth strata, with a horizontal extent of approximately 28 m and a maximum depth of about 10 m. On the right slope, the critical slip surface had a horizontal span of around 42 m and a maximum depth of 40 m. The significantly higher safety factor of the right slope could be attributed to the protective effect of the rock basin structure in the framed reef tuff, which safeguards the middle-inner reef apron. Additionally, the right slope predominantly consisted of the fifth stratum, where the framed reef tuff exhibited superior lithological properties.
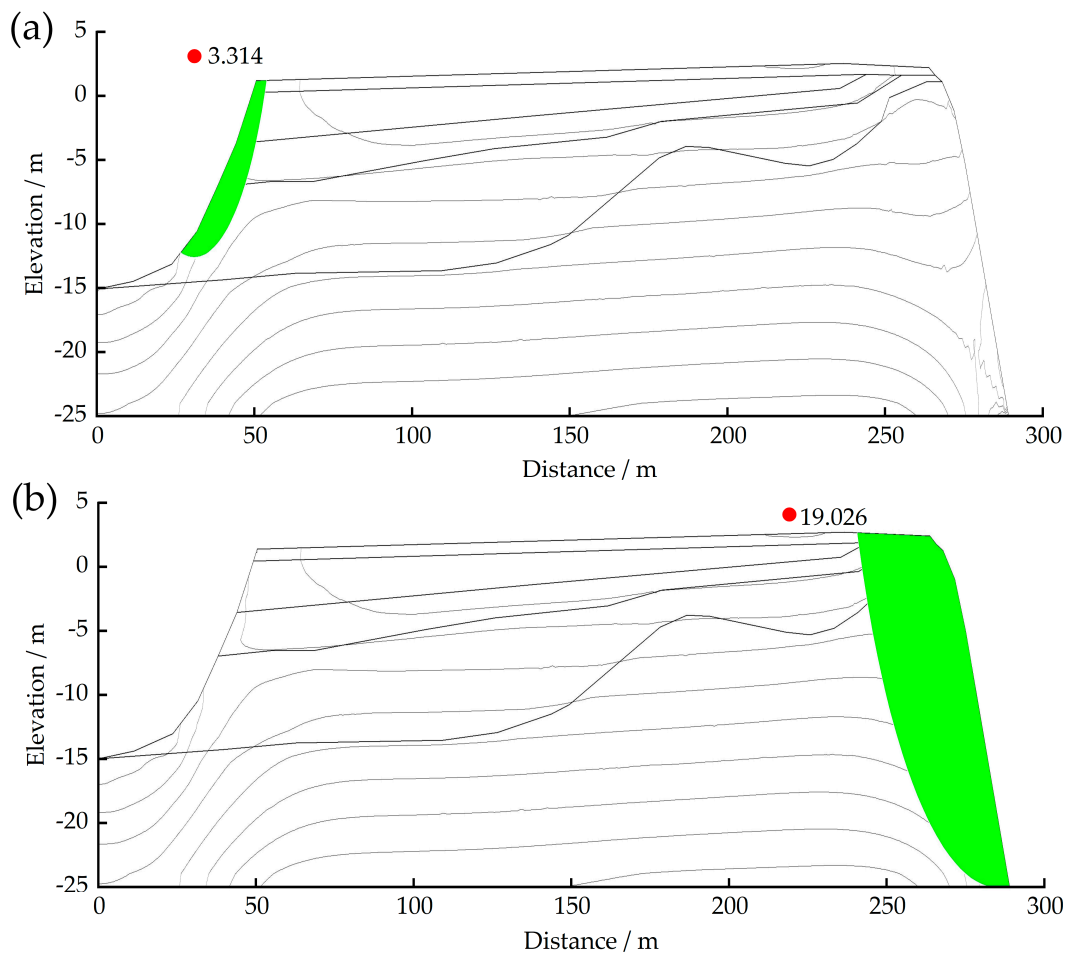
Figure 5. Potential slip surfaces and safety factors of slopes on both sides under self-weight condition. (**a**) Left slope; (**b**) right slope. Note: Safety factors of the slopes are marked in the figure. The green areas represent the critical slip surfaces.

4.1.2. Probabilistic Stability Analysis of the Slope Under Static Conditions

Previous studies have highlighted that the development of coral reefs is characterized by cyclonic deposition and tower-like layering. This unique geological structure results in significant spatial heterogeneity and stochasticity in their geotechnical properties. Due to the complexity of the depositional environment and variations in later diagenesis, the material parameters (e.g., cohesion and internal friction angle) of different layers within coral reefs can exhibit considerable variability across different spatial locations. The variability of these parameters directly impacts the reliability of stability analysis results. In this study, a normal distribution was used to describe the probability distribution of effective cohesion and effective friction angle for each stratum, with the design values of the distributions provided in Table 3. Xu et al. [2], Zhu et al. [3], and Wang et al. [24] have conducted detailed and effective research on the mechanical properties of reef limestone and coral sand. The design values adopted in this study are derived from a comprehensive review and synthesis of previous research and geological data.

Table 3. Cohesion and friction probability distribution settings.

Stratum	Standard Deviation		Input Range	
	Cohesion/kPa	Friction Angle/°	Cohesion/kPa	Friction Angle/°
1	5	5	5–30	5–25
2	2	5	0–8	20–40
3	6	6	14–26	18–35
4	5	5	0–30	15–30
5	200	4	1000–1400	30–42

The results (Figure 6) show that the maximum and minimum safety factors for the left-side slope of the model were 2.393 and 5.379, respectively, with a mean value of 4.187. The frequency distribution was concentrated in the range of 3.6–4.4. For the right-side slope, the maximum and minimum safety factors were 16.293 and 22.834, respectively, with a mean value of 19.49. The frequency distribution was somewhat more dispersed compared to the left-side slope, primarily concentrated in the range of 17.6–21. The calculation results indicate that the probability of instability for both slopes under static conditions was P_f = 0%.
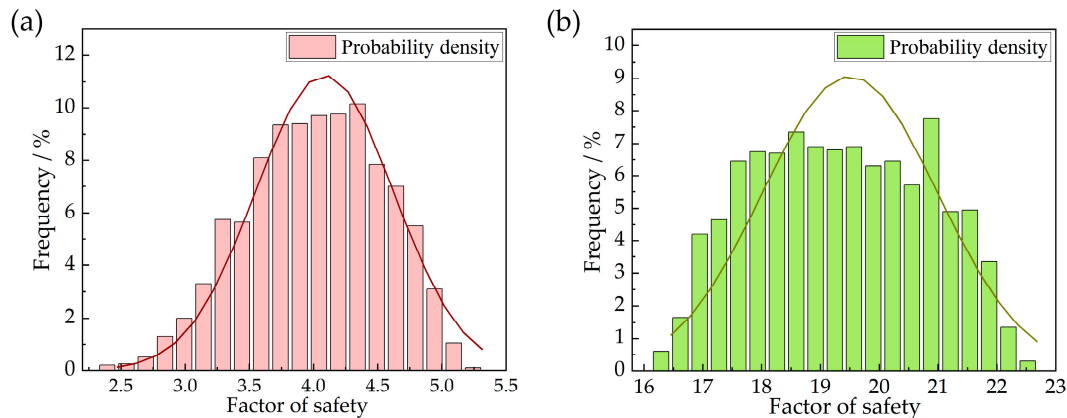
Figure 6. Probability density function and normal curve of the model slope safety factor. (**a**) Left slope; (**b**) right slope.

4.2. Stability of Reef Body Slopes Under Different Seismic Intensities

4.2.1. Slope Safety Factor

Through static analyses, this study reveals the stress distribution characteristics of the reef body under self-weight conditions and evaluates the stability of the side slopes on both sides. The results indicate that, under static conditions, the overall stability of the reef body was relatively high. However, the stability of the left slope was comparatively weaker, making it more susceptible to external loads. In practical engineering environments, the reef body is not only subjected to self-weight and water pressure but may also experience significant impacts from natural disasters such as earthquakes. Seismic effects can trigger the redistribution of internal stresses within the reef body, induce cumulative deformation and potential sliding, significantly reduce the slope safety factor, and even lead to destabilization and damage. Therefore, it is essential to conduct further dynamic analyses to investigate the stability characteristics of the reef body and its evolution under seismic effects of varying intensities. As a random event, earthquake intensity and peak ground acceleration (PGA) exhibit high uncertainty and a wide range of distribution. In this study, we selected six artificial seismic waves with PGA values ranging from 0.05 g to 0.4 g. According to the Modified Mercalli Intensity (MMI) [32] scale and the classification by the United States Geological Survey (USGS), a PGA of 0.05 g corresponds to a light

earthquake, 0.1 g to a moderate-intensity earthquake, 0.2 g to a moderately strong earthquake, 0.3 g to a strong earthquake, and 0.4 g to a very strong earthquake. This range of intensities essentially covers the spectrum from light to very strong earthquakes, providing a representative sample for analysis. The stability of the slopes was comprehensively assessed in terms of stresses, permanent displacements, and the factor of safety.

Firstly, the Quake/W module was used to apply seismic wave loads to the model to obtain the response results for the reef body model. The Newmark method was then used to calculate the factor of safety for the side slopes during the seismic process, as well as to determine the permanent displacement of the model. Figure 7a presents the values of the minimum factor of safety for the side slopes on both sides of the reef body under different peak acceleration earthquakes. According to the simulation results, the side slopes of the coral reef body exhibited noticeable stability differences under seismic waves of varying intensities. The minimum factor of safety for both the left- and right-side slope decreased linearly as seismic intensity increased. The left-side slope showed slightly higher sensitivity to seismic load than the right-side slope. Under the impact of an earthquake exhibiting a peak ground acceleration (PGA) of 0.4 g, the minimum factor of safety for the left-side slope decreased by 75% compared to the initial value (the initial factor of safety under static conditions was 3.314 for the left slope), while the right-side slope's minimum factor of safety decreased by 68.4% (the initial factor of safety under static conditions was 19.028 for the right slope). For the right slope, the minimum factor of safety dropped to 6.355 under the PGA 0.4 g seismic wave, but it remained significantly higher than the critical value (FOS = 1.0), indicating no risk of failure. For the left slope, the minimum factor of safety approached the critical instability value under the PGA 0.3 g seismic effects and dropped below the critical value under the PGA 0.4 g seismic wave effects (0.804). However, during the seismic process, the factor of safety of the slope was above the critical value for most of the time, meaning that the slope remained stable for the majority of the event. This suggests that using only the traditional instability criterion to evaluate stability may not be sufficient. In this study, the minimum average factor of safety index was introduced; Liu et al. [33] pointed out that incorporating the minimum average safety factor provides a more comprehensive evaluation of slope stability under seismic effects. The minimum average safety factor was calculated as the initial safety factor minus 0.65 times the difference between the initial safety factor and the minimum safety factor. Slope stability was comprehensively evaluated by combining the traditional criterion, the minimum average factor of safety, and permanent displacement.

The results for the minimum average factor of safety are shown in Figure 7b. The decreasing trend in the slope's factor of safety aligns with the decline in the minimum factor of safety. Under the highest-intensity earthquakes in this analysis, the left- and right-side slope have decreased by 48.7% and 42.1%, respectively. However, the minimum average safety factor of the reef slope remained above the critical instability value under all seismic conditions. For the left slope, the minimum average safety factor under the six seismic intensities (from weak to strong) ranged from 1.6 to 2.7 times the critical value. For the right slope, the minimum average safety factor under the same range of seismic intensities ranged from 10.9 to 17.1 times the critical value. This indicates that, overall, the slope's stability was slightly higher than the critical instability threshold during the seismic event and remained in a stable state. Nevertheless, the risk of instability during the peak acceleration intervals of the seismic event should be carefully considered and analyzed.
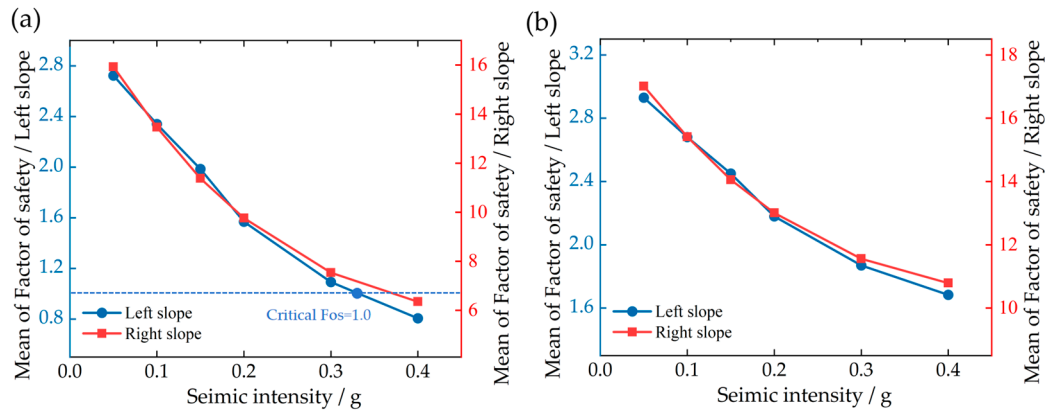
Figure 7. Slope safety factors of the reef body under different seismic intensities. (**a**) Minimum safety factor; (**b**) minimum average safety factor.

4.2.2. Stress Field and Displacement Field

According to the trend of the reef body's slope safety factor during seismic influence, the lowest safety factor occurred at the 2.4-s mark of the 0.4 g PGA seismic wave. The effective stress distribution within the reef body effectively reflected the impact of the earthquake on the reef (shown in Figure 8). In this study, we extracted the effective stress distribution and the instantaneous displacement field distribution of the reef body at the moment when the lowest safety factor was observed. Under the seismic influence, the effective stress within the left lagoon slope showed significant changes, with the horizontal effective stress increasing notably compared to static conditions. This indicates a certain risk of instability for the lagoon slope at that moment.

Figure 8b shows the displacement distribution at the 2.4-s mark. It can be observed that the larger displacement area was concentrated at the foot of the slope, located in Stratum 5. This is because, as the earthquake reaches its peak intensity, the basal part of the model experiences a concentration of shear stresses, resulting in a larger displacement response and relatively high shear deformation in this area. This is a key factor contributing to the decrease in the safety factor. However, the results indicate that the maximum instantaneous displacement of the model at this moment is 6.56 cm. Griffith et al. [34] noted that for most geotechnical structures, an instantaneous displacement of less than 10 cm is generally considered acceptable, posing no significant threat to slope stability and unlikely to trigger large-scale sliding or failure. Therefore, the occurrence of instability requires further analysis and evaluation.
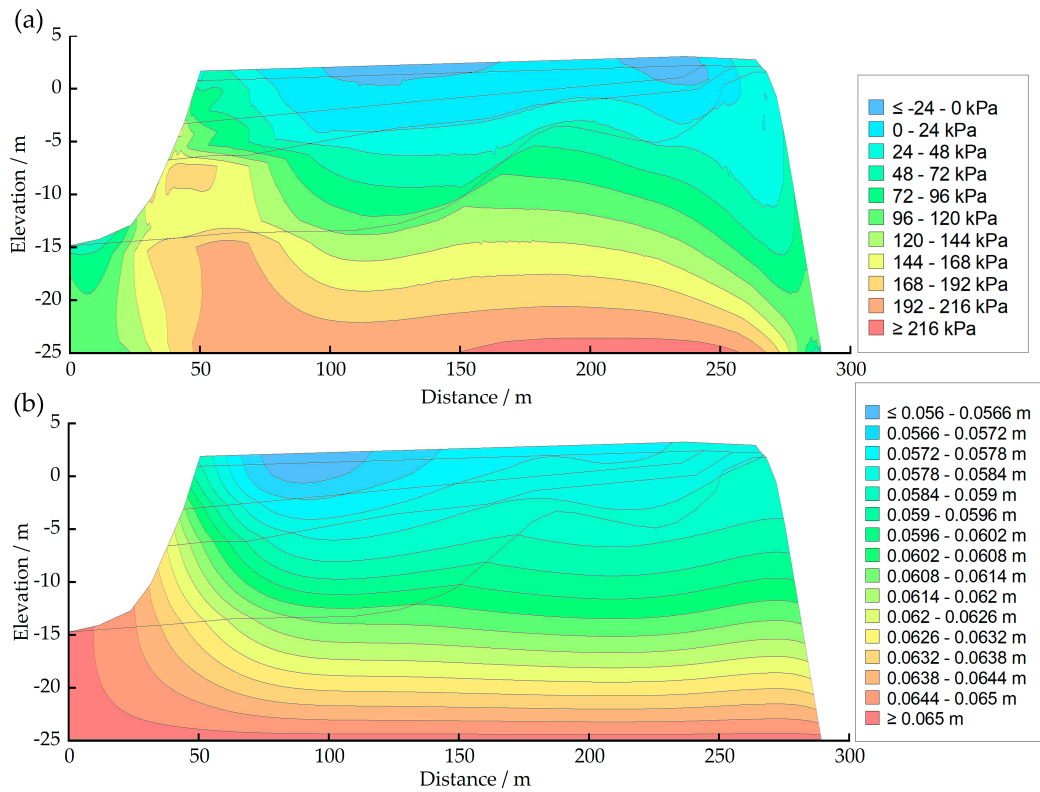
Figure 8. Distribution of horizontal effective stress field and displacement at 2.4 s of the PGA 0.4 g earthquake; (**a**) horizontal effective stress; (**b**) displacement.

The horizontal effective stress and maximum shear stress of the slope were monitored longitudinally at a distance of 50 m in the horizontal direction, as shown in Figure 9. It can be observed that both the horizontal effective stress and the maximum shear stress significantly increased during the seismic process. At 2.4 s, the shear strength of the soil strips at the 50 m horizontal distance was approximately 120 kPa. Combining this with Figure 9a below, it is evident that the maximum shear stress of the soil strip at an elevation of −11 m exceeded the shear strength at 2.4 s, indicating a risk of slippage. Figure 10 shows the critical slip surface at the most dangerous moment during the PGA 0.4 g earthquake. The critical slip surface penetrated all strata except the framework reef limestone, with a horizontal span of approximately 100 m.
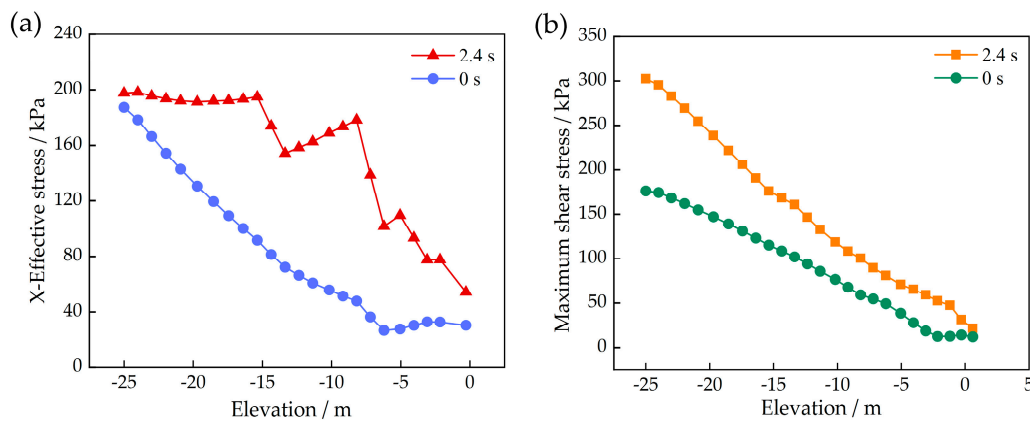
Figure 9. Relationship between horizontal effective stress, maximum shear stress, and depth at X = 50 m at 2.4 s of the earthquake; (**a**) horizontal effective stress; (**b**) maximum shear.
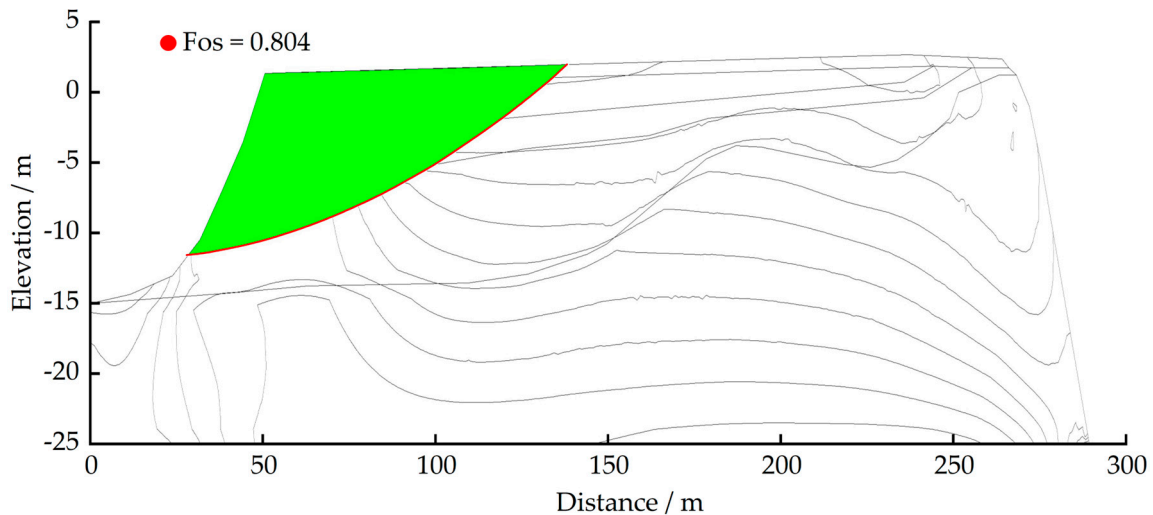
Figure 10. Distribution of the most dangerous slip surface at 2.4 s.

4.2.3. Permanent Displacement

Using the Newmark method, the permanent displacement of the critical slip surface can be obtained through integration, which serves as an important criterion for slope stability assessment. Regarding the correlation between slope instability and permanent displacement, as well as the criteria for evaluating permanent displacement, extensive research has been conducted by previous researchers [28,35].

The computational results of the dynamic response under six different PGAs indicated that the coral reef slope model did not exhibit permanent displacement under seismic scenarios with PGAs of 0.05 g, 0.1 g, 0.15 g, and 0.2 g. This indicates that the reef body remained relatively stable under earthquakes with PGA up to 0.3 g. In contrast, under a PGA 0.3 g earthquake, the left-side slope experienced a permanent displacement of 1.12 cm at the critical slip surface at the most hazardous moment. Under a PGA 0.4 g intensity earthquake, the left-side slope experienced permanent displacements at the critical slip surface during the seismic process, specifically between 2 and 2.4 s, between 3.8 and 4.1 s, and again at 9 s. The most hazardous slip surface, identified in the conventional analysis at 2.4 s, eventually produced a permanent displacement of 0.6 cm. This suggests that, although we observed a lower instantaneous safety factor at 2.4 s, it did not necessarily imply that a landslide occurred. Additionally, during the earthquake, the slip surface with the maximum permanent displacement produced a displacement of 3.8 cm. The distribution of this maximum permanent displacement slip surface is shown in Figure 11. The horizontal span of this slip surface was smaller than that of the slip surface with the lowest safety factor, but its depth was greater, penetrating approximately 15 m. This also indicates that the framework reef limestone stratum did not experience any permanent displacement. All potential slip surfaces collectively produced a total permanent displacement of approximately 25.4 cm during the earthquake. Jibson et al. [28] stated that displacements between 2 and 15 cm may cause small-scale landslides. Jibson and Michael et al. [35] used permanent displacement values to assess the probability of damage: displacements between 0 and 1 cm correspond to a low probability, between 2 and 5 cm to a medium probability, and greater than 5 cm to a high probability of landslides. The results of permanent displacement indicate that the slope faces a moderate risk of landslide damage.
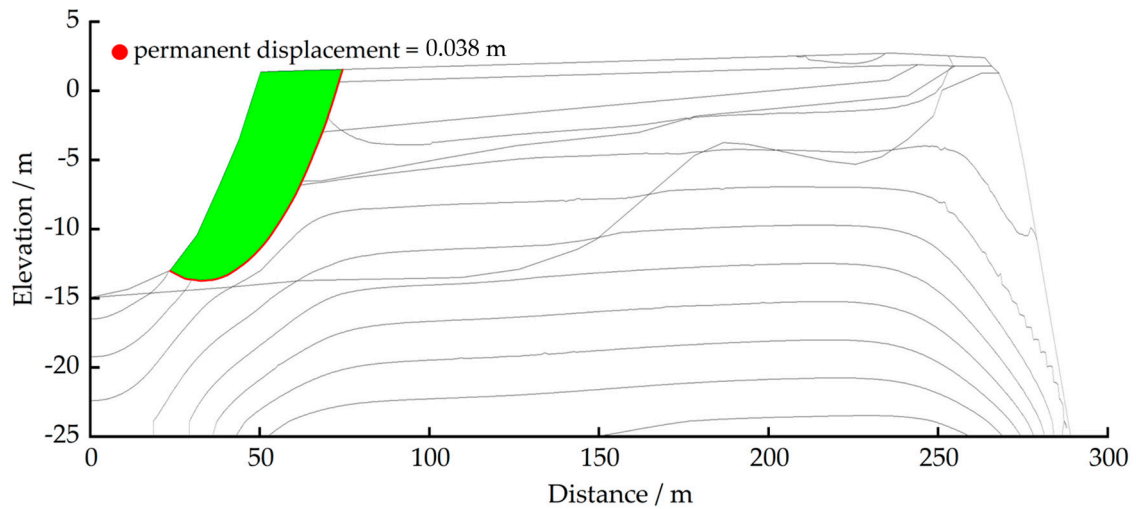
Figure 11. Maximum permanent displacement slip surface under PGA 0.4 g seismic influence.

4.2.4. Probabilistic Stability of Reef Body Slopes Under Seismic Influence

In order to further analyze the effect of earthquakes on the slope stability of the reef body and assess the potential for landslide damage on the critical slip surface during the seismic process, the finite element method was utilized to conduct probabilistic stability analysis of the reef body's dynamic response. The probability distributions were primarily reflected in the heterogeneous distribution of effective cohesion and effective friction angle across the various strata. The calculation parameters were set with the same distribution settings as in the static conditions, as shown in Table 3.

Consistent with the conventional analysis, the probabilistic stability analysis of the right-side slope of the reef indicates that the right-side slope was more stable under seismic influences due to the protective effect of the framed reef tuff basins, making landslides and damage highly unlikely. Therefore, this section focuses on analyzing the probabilistic stability of the left-side slope. Figure 12a illustrates the time-course curves of instability probability and maximum instability probability under the influence of the PGA 0.3 g earthquake. The destabilization probability refers to the likelihood of destabilization failure for a specific critical slip surface at each time point up to a certain moment in the reef body slope model, while the maximum destabilization probability represents the probability of failure for the slip surface with the lowest instantaneous stability at a given time point. Under this seismic intensity, the maximum instability probability and the critical slip surface instability probability were essentially overlapping, with the maximum instability probability being slightly higher than the critical slip surface instability probability at 2.12 s. At 2.4 s, the maximum instability probability was slightly greater than the critical slip surface instability probability. At this moment, the factor of safety of the left slope was estimated to be 1.05, still above the critical value, but a maximum instability probability of 48.2% occurred.
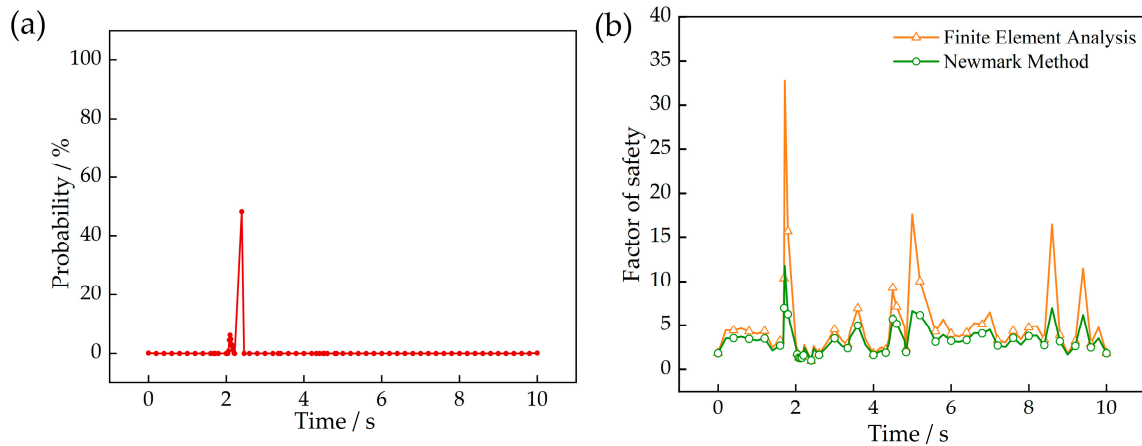
Figure 12. Instability probability and safety factor time-course of the left-side slope under the influence of the PGA 0.3 g earthquake; (**a**) Time-history curve of instability probability; (**b**) Time-history results of safety factors from the probabilistic stability analysis method and the Newmark method.

Under the influence of the PGA 0.4 g seismic wave, the results show that the highest probability of instability, 100%, occurred during the time period from 2.0 to 2.4 s, which aligns with the most hazardous moment identified in the traditional analysis (shown in Figure 13). The above computational results are based on the model assumptions established in this study; however, the extremely high instability predictions also indicate that the coral reef multi-layered slope site faced a significantly high risk of damage under seismic conditions with a PGA greater than 0.4 g. The left slope, under the seismic intensity of PGA 0.4 g, reached its peak sliding damage during this period (the slip surface is shown in Figure 10 of Section 4.2.2). Figure 14 illustrates the probability density function and the normal distribution curve of the slope safety factor at the most critical moment during an earthquake with a peak ground acceleration of 0.4 g.
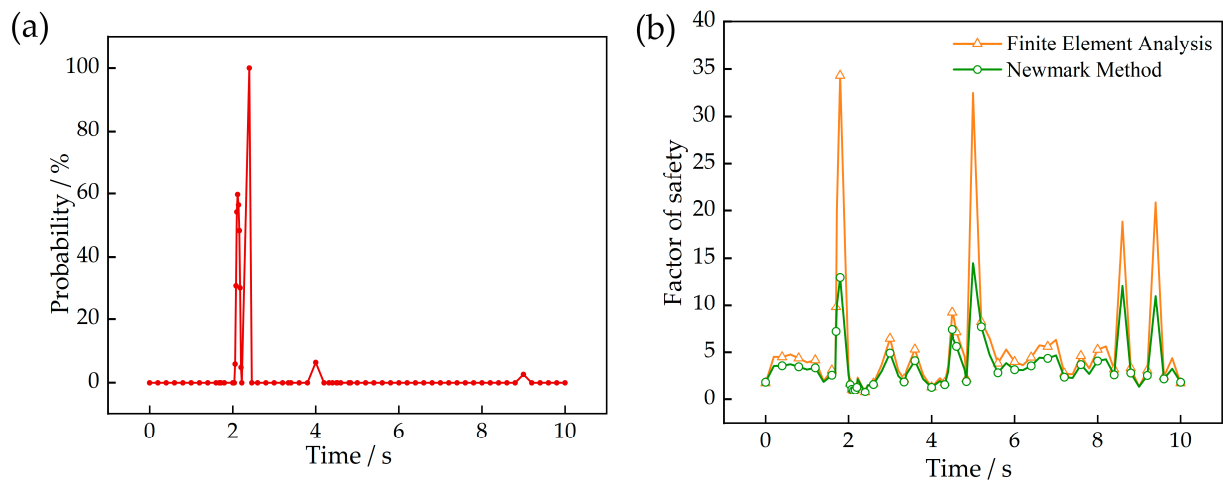
Figure 13. Instability probability and safety factor time-course of the left-side slope under the influence of the PGA 0.4 g earthquake; (**a**) Time-history curve of instability probability; (**b**) Time-history results of safety factors from the probabilistic stability analysis method and the Newmark method.
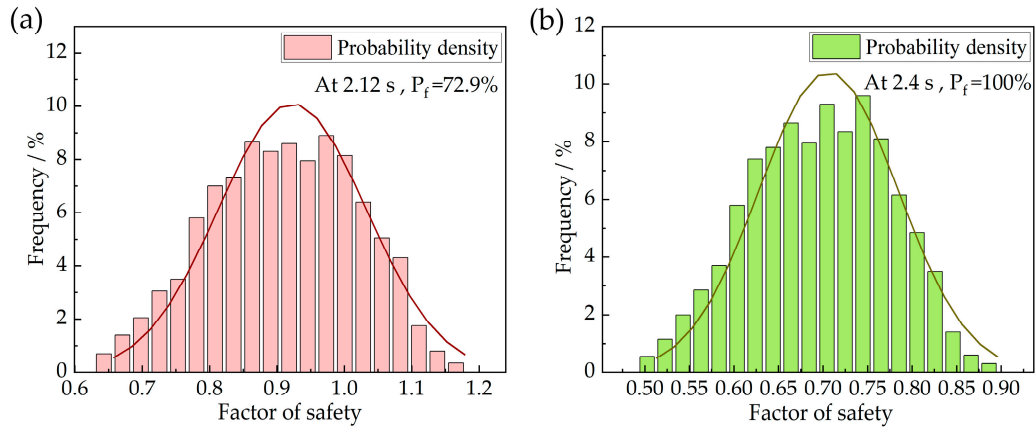
Figure 14. Probability density function and normal curve of slope safety factor at the hazardous time points under the PGA 0.4 g earthquake (P_f is the instability probability). (**a**) At 2.12 s; (**b**) at 2.4 s.

4.3. Stability of Reef Body Slopes Under Extreme Seismic Conditions

In order to further assess the stability of reef body slopes under extreme seismic conditions, this paper introduced an actual observed seismic wave (shown in Figure 15) as an input load, building on analyses conducted using synthetic seismic waves. This study selected the 1995 Kobe earthquake wave as the extreme condition seismic wave, which is characterized by long duration and extreme intensity. It was extracted from actual monitoring data and represents the characteristics of strong earthquakes in seismically active regions. The Kobe earthquake wave features multi-frequency components and long duration, enabling it to more accurately reflect the complex ground motion characteristics under strong seismic conditions. Compared to typical synthetic seismic waves, the use of the Kobe earthquake wave better captures the uncertainty and complexity of seismic loading in real earthquake events, such as the time-history characteristics of peak ground acceleration and the impact of multi-frequency properties on slope stress distribution and permanent displacement. Synthetic seismic waves, typically based on simplified source models and site conditions, may not fully capture the multi-frequency and non-stationary characteristics of actual earthquakes [36].

This seismic wave has several characteristics that distinguish it from the artificial wave: first, it has a long duration, which allows for effective simulation of extreme seismic conditions; second, its peak acceleration range encompasses the acceleration values investigated in the preliminary analysis of this paper; and third, it can represent the ground shaking characteristics of oceanic regions to some extent. By introducing real seismic waves, a more comprehensive exploration of the response characteristics and potential instability mechanisms of reef slope stability at different time points under extreme seismic conditions can be achieved.
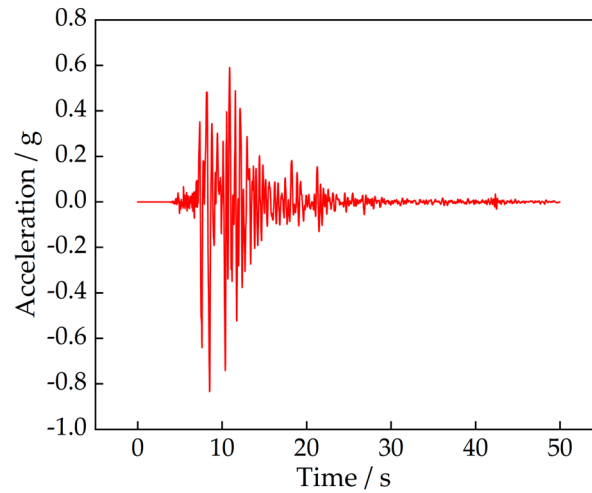
Figure 15. Acceleration time-history of the actual observed seismic wave.

Based on the simulation results, Figure 16 shows the time-course curves of the slope safety factor for both sides of the reef under the influence of actual seismic waves. The safety factor was significantly affected by the earthquake, with the safety factor of both slopes decreasing to its lowest value during the peak acceleration interval of the earthquake. The lowest FOS for the left slope was 0.41, occurring at 10.86 s, while the lowest FOS for the right slope was 2.595, occurring at 11.78 s. Correspondingly, the average FOS for the left slope was 1.426, and the average FOS for the right slope was 8.34.
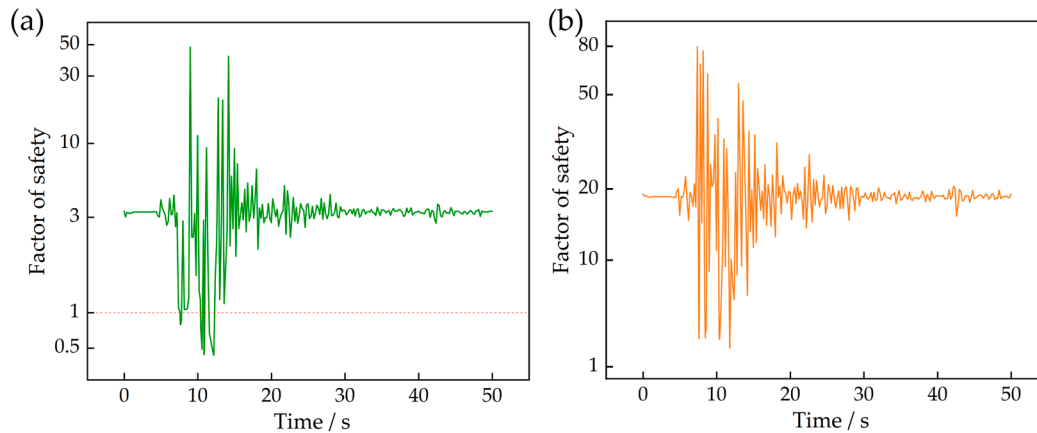
Figure 16. Slope safety factor time-course curves of the reef body. (**a**) Left slope; (**b**) right slope.

The permanent displacement caused by the earthquake was calculated while using the Newmark method to determine the effect on the safety factor. The results showed that the acceleration response value of the right-side slope under the influence of this seismic wave did not exceed the critical acceleration, and no permanent displacement occurred. We focused on analyzing the cumulative permanent displacement characteristics of the left slope. Due to the multi-frequency components and long duration of the observed Kobe seismic wave, comparing its displacement patterns with those generated by synthetic seismic waves can provide clearer insights into permanent displacement analysis. Therefore, we synthesized an artificial seismic wave with the same peak ground acceleration (PGA) as the Kobe wave and analyzed the cumulative permanent displacement characteristics of the left slope under seismic influence, combined with a PGA 0.4 g seismic wave. The results show that under the influence of the Kobe wave, the left slope accumulated approximately 2.5 m of permanent displacement. Under the influence of the artificial wave with PGA 0.83 g, the cumulative permanent displacement was about 1.3 m, while under

the influence of the artificial wave with PGA 0.4 g, the cumulative permanent displacement was 0.038 m (Shown in Figure 17).
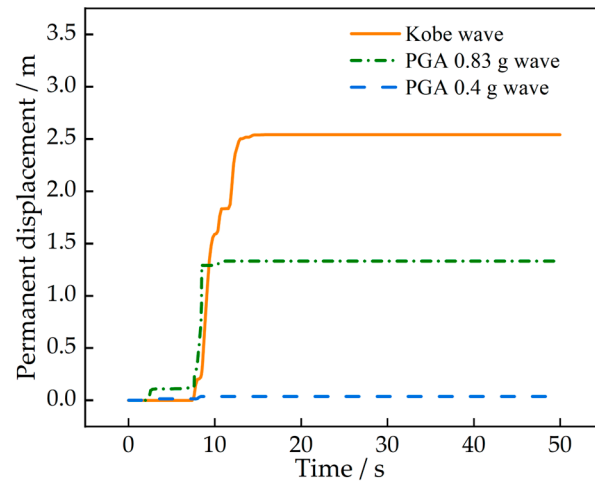
Figure 17. Time-history curves of cumulative permanent displacement for the left slope under the influence of three different seismic waves.

5. Discussion

5.1. Effect of Stratified Structure on the Static Stability of Slopes

The stability analysis under self-weight conditions primarily focuses on two aspects: the distribution of internal effective stress and the evaluation of the slope safety factor of the reef body. The results of the horizontal stress distribution inside the reef body show the horizontal stress within the reef body exhibited a relatively uniform distribution, with lower stress values in most areas, indicating a relatively small horizontal load inside the reef. Tensile stress in the shallow regions of the reef body may pose a potential threat to the stability of the stratigraphic structure. It was observed that the first and second strata on the reef surface were primarily subjected to tensile stress in the middle and inner reef apron areas, with low stress values (<0.02 MPa). In the outer area of the middle reef apron, tensile stress values exceeded 0.02 MPa but remained below 0.04 MPa in a small, localized region. Wang et al. [14] reported that the dry average tensile strength and saturated tensile strength of the coral reef apron conglomerate rock layer are 1.21 MPa and 1.14 MPa, respectively. These values are significantly higher than the calculated tensile stress values in the tensile stress zones, indicating that the tensile stresses on the reef surface had a negligible effect on the overall structural stability and were insufficient to produce tensile cracks. The horizontal effective stresses from the third to fifth strata gradually increased with depth and exhibited a more uniform distribution, reflecting greater stress stability in the deeper strata. The vertical effective stress distribution is shown in Figure 5b. It displays an obvious linear increasing trend, consistent with the effect of self-weight. The maximum vertical stress reached 650 kPa, with a well-uniform stress distribution. No tensile stress was observed in the surface layer, indicating strong overall stability of the reef structure. Additionally, the vertical effective stress in the right half of the reef was slightly higher than in the left half. This difference is attributed to the greater unit weight of the tuff strata in the framed reef and the topographic elevation difference on the right side. While this variation may influence local stresses, it did not significantly impact the overall stability of the reef body.

Slope stability is a critical indicator for assessing the overall stability of a reef body. This study evaluated the safety factors of the slopes on both sides of the reef body. According to the analysis results, there was a significant difference in stability between the

left and right slopes. The critical slip surface of the left slope spanned from the first to fourth strata, with a horizontal length of approximately 28 m and a maximum depth of about 10 m. The safety factor was evaluated to be 3.314, which was significantly lower than that of the right slope but still exceeded the destabilization threshold by 331%. This indicates that the left slope remained stable under self-weight conditions. In contrast, the critical slip surface of the right slope spanned about 42 m horizontally and reached a maximum depth of 40 m. Its safety factor was as high as 19.028, indicating remarkable stability. The marked disparity in stability between the two slopes can be attributed to differences in the properties of their constitutive strata. The shallow surface strata (Strata 1–4) on the left slope were composed of looser materials, such as bioclastic sand and chalk, with lower shear strengths, making them more susceptible to the influence of potential slip surfaces. Additionally, the surface rock and soil layers of the reef transitioned from strong cementation characteristics on the seaward side to weaker cementation on the lagoon side. This resulted in a more loosely consolidated soil structure on the lagoon-side slope, with significantly weaker stability and seismic performance compared to the seaward-side slope, as reflected in the safety factor, where the lagoon-side slope's safety factor was much lower than that of the seaward-side slope. In comparison, the framework reef limestone of Stratum 5 constituted the main part of the right slope. Compared to other strata, the framework reef limestone exhibited superior mechanical properties, such as unit weight, shear strength, and cohesion, which contributed to the stability of the slope. Additionally, for the right slope, the overall geometry of Stratum 5 presented a basin-like structure, with higher elevation on the outer side and lower elevation on the inner side. This configuration provided a certain degree of protection to the right slope. Moreover, the inward-dipping trend of Stratum 5 opposed the potential sliding direction of the right slope, thereby mitigating the sliding tendency under both static and seismic conditions. In summary, the presence of Stratum 5 significantly enhanced the stability of the right slope. Combined with the stability analysis of the coral reef slope under dynamic loading, the seismic impact also caused a significant decrease in the stability of the right slope. However, due to the excellent mechanical properties of the framework reef limestone and the protective effect of the basin-like structure of Stratum 5 on the right slope, the safety factor of the right slope remained well above the critical instability threshold under all six artificial seismic wave scenarios considered in this study. This is consistent with the view of Tang et al. [11], who suggested that the significant difference in safety factors between the outer and inner slopes of the reef can be attributed to the "layered cake" structure of the lagoon-side reef slope and the "block cake" structure of the offshore reef slope. The large difference in safety factors between the outer and inner slopes indicates that, even when wave action and earthquakes are considered as the main external influencing factors in actual engineering, the stability of the reef is primarily determined by its physical properties. The static probabilistic stability analysis showed that the failure probability of the slopes on both sides was 0%, which is consistent with the safety factor assessment. This calculation result was based on the basic assumptions of the multi-layer coral reef limestone slope dynamic response stability evaluation model established in this study.

In summary, this study concludes that both side slopes of the reef body model were stable under self-weight conditions, with a low risk of landslide damage. However, the stability of the left slope was significantly lower than that of the right slope due to the presence of shallow loose sediments. This made the left slope a weak point and a key focus in the stability assessment of the reef.

5.2. The Impact of Different Seismic Intensities on the Stability of Coral Reef Bodies

The focus of the dynamic analysis is to explore how the transient and cumulative effects induced by seismic activity influence the stability of the reef body, as well as the

differences in the response of the side slopes under seismic loads of varying intensities. Based on the simulation results for different seismic intensities, this paper provides a detailed analysis of the stress changes, time-dependent characteristics of the safety factor, and the slip trends within the reef body, aiming to assess the extent of seismic effects on the reef's stability. In this study, the stability of the reef is primarily analyzed and evaluated in terms of the slope safety factor, stress distribution within the reef, permanent displacement, and other relevant factors. Table 4 is presented the main results of the slope safety factor from the dynamic response analysis.

Table 4. Slope safety factor under the influence of different seismic intensities.

PGA/g	Fos of Left Slope		Fos of Right Slope	
	Minimum	Mean	Minimum	Mean
0.05	2.723	2.929	15.928	17.012
0.1	2.34	2.680	13.465	15.411
0.15	1.985	2.450	11.379	14.055
0.2	1.569	2.179	9.764	13.005
0.3	1.092	1.869	7.538	11.558
0.4	0.806	1.683	6.355	10.789

Under seismic action, the safety factor of the reef slope was significantly affected. Analyzing the safety factor values for the left- and right-side slope under six different seismic intensities revealed a clear decreasing trend in the minimum safety factor as seismic intensity increases. The right-side slope experienced a relatively small decrease in safety factor due to the high lithology of the framed reef tuff, which had strong anti-slip properties, maintaining a level much higher than the critical destabilization value. In contrast, the left-side slope was more sensitive to changes in seismic intensity due to the presence of more weak overlying layers. Specifically, under high-intensity earthquakes with peak accelerations of 0.2 g or higher, the safety factor of the left-side slope rapidly approached the critical value for instability. Ultimately, the minimum safety factor fell below the critical destabilization value under earthquakes with peak accelerations of 0.4 g. Slope stability was also assessed in terms of the side slope stability, which plays a crucial role in the overall stability evaluation. Moreover, as a key criterion for assessing slope stability, the decreasing trend of the average safety factor for the reef body slopes, in response to increasing seismic intensity, mirrored that of the minimum safety factor. However, both values remained above the critical destabilization threshold. Seismic waves were characterized by high acceleration loads during short peak periods, followed by relatively low acceleration loads for most of the duration. Although the overall slope stability did not significantly decrease, the slopes remained at high risk during peak seismic acceleration events. The shear modulus of the fifth stratum in this model was significantly higher than that of other strata, which could potentially lead to stress concentration and instability. Therefore, we focused on the distribution of shear stress and shear strain under the PGA 0.4 g seismic peak dynamic load, as shown in Figure 18. It was observed that no stress concentration occurred in the slope under dynamic loading, indicating that the difference in shear modulus between the fifth stratum (720 MPa) and the fourth stratum (500 MPa) was insufficient to induce stress concentration under dynamic loading. The shear strain distribution revealed strain concentration at the interface between the fourth and fifth strata. However, this area had a gentle slope, close to horizontal, so the potential failure surface under dynamic loading did not intersect this region. Therefore, it was essential to incorporate permanent displacement analysis and probabilistic stability analysis to focus on these critical aspects.
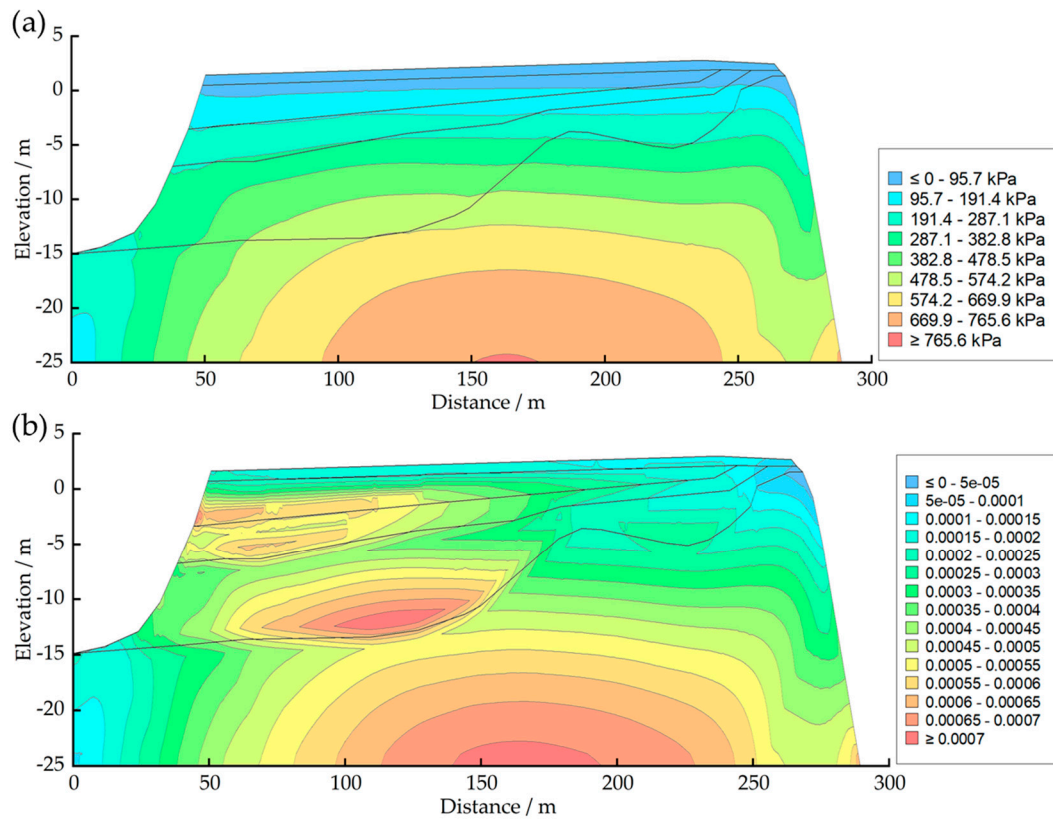
Figure 18. (**a**) Shear stress distribution of the reef under peak ground acceleration; (**b**) shear strain distribution of the reef under peak ground acceleration.

In this study, the maximum permanent displacement of the slip surface was selected as the evaluation criterion for assessing the instability risk of the slope. According to the results of the permanent displacement calculations, no permanent displacement occurred on the right-side slope under any of the working conditions. For the left-side slope, under seismic conditions with a PGA of 0.3 g, no permanent displacement occurred. However, under the same seismic condition, the critical slip surface experienced a permanent displacement of 1.12 cm. When the seismic intensity reached a PGA of 0.4 g, the critical slip surface experienced a permanent displacement of 3.8 cm. Jibson et al. [28] stated that displacements between 2 and 15 cm may cause small-scale landslides. Jibson and Michael et al. [35] used permanent displacement values to assess the probability of damage: displacements between 0 and 1 cm correspond to a low probability, between 2 and 5 cm to a medium probability, and greater than 5 cm to a high probability of landslides. Griffith et al. [34] proposed a displacement-based method for slope stability assessment and validated the applicability of permanent displacement thresholds in slope stability analysis. They also emphasized that the selection of permanent displacement thresholds should consider the geometric characteristics of the slope, material properties, and seismic loading conditions. For different types of slopes, the range of permanent displacement thresholds may vary but typically falls within a few centimeters to several tens of centimeters. Duncan et al. [29], through extensive experimental and numerical simulations, investigated the permanent displacement characteristics of slopes under complex geological conditions. They proposed permanent displacement evaluation criteria suitable for different geological conditions and discussed the impact of displacement thresholds on slope stability. They pointed out that for coral reef slopes, due to their high porosity and anisotropy, the permanent displacement thresholds should be lower than those for traditional terrestrial soils. Therefore, the permanent displacement evaluation standard adopted in this study, based on the criteria for terrestrial geotechnical materials, ensures that the seismic impact

on slope stability is not underestimated. Based on this, this study concludes that there is no risk of destabilization for the reef body slopes subjected to seismic loads with a peak acceleration of less than 0.3 g. The risk of destabilization for the reef body slopes subjected to seismic loads with a peak acceleration of 0.3 g is low, while the risk is medium-high for slopes subjected to seismic loads with a peak acceleration of 0.4 g.

To further investigate the risk of slope instability of the reef body under seismic loading and the probability of slope failure at critical moments during the seismic process, a probabilistic stability analysis was introduced in this paper. Probabilistic stability analysis of the slope was achieved by combining the finite element method with the slope stability method. The finite element model and its assumptions remained consistent with the original model. As shown in Figure 13b, the time-history curve of the safety factor derived from both methods shows a high degree of consistency in terms of the overall trend and the minimum value of the safety factor. However, the finite element method resulted in a significantly higher average safety factor compared to the Newmark method. While both methods follow the same trend for most of the time, the finite element method better reflects the instantaneous dynamic effects, whereas the Newmark method tends to focus more on the overall stability. The finite element method is based on the theory of continuous medium mechanics and calculates the safety factor by analyzing the stress–strain distribution within the slope soil body. It considers the overall response of the slope under seismic loading, particularly capturing local stress concentrations and deformation tendencies. On the other hand, the Newmark method is a simplified rigid-body sliding model that assumes a rigid slip surface and neglects the complex stress and deformation characteristics within the slope when calculating the sliding force. The finite element method is more sensitive than the Newmark method, and the differences in the results highlight the finite element method's higher sensitivity to local stress concentrations and the dynamic response of the slope. The results from the Newmark method were relatively smooth, primarily reflecting the cumulative effects of the sliding force. The very high safety factor values that appeared several times were due to transient stability enhancements caused by small dynamic forces at specific moments and local stress release on the slope.

The results of the probabilistic stability analyses indicate that the right-side slope showed no risk of instability under all seismic conditions, demonstrating good stability and seismic performance. For the left-side slope, the probability of instability under low-intensity seismic conditions was 0%, meaning that the slope dod not exhibit any instability tendencies under seismic action. This suggests that the side slopes remained highly stable under weaker seismic loads, with a low risk of instability. When the seismic intensity reached a PGA of 0.3 g, the probability of instability of the left-side slope increased to 48.2%, indicating a significant rise in the likelihood of slope instability. Under these conditions, the potential destabilization area of the slip surface had significantly expanded, although the slope still retained some seismic capacity. This phenomenon suggests that the increase in seismic intensity began to trigger stress redistribution within the reef body, sharply raising the risk of localized instability on the left-side slope. Under the strong seismic condition of a PGA of 0.4 g, both the probability of instability and the maximum probability of instability of the left slope reached 100%, indicating that the slope was already in an unstable state under this high seismic loading. Based on the assumptions of the computational model in this study, the instability probability reached 100% under seismic impacts with a PGA of 0.4 g or higher. Combined with the permanent displacement analysis results and the permanent displacement evaluation criteria, the slope under these conditions also faced a high risk of failure. This indicates that for coral reef multi-stratum slopes in such areas, earthquakes with a PGA above 0.4 g significantly affect slope stability, with a very high probability of failure. The seismic capacity of the slope is

entirely weakened, and instability becomes almost inevitable. According to Duncan et al. [29], the installation of anchors or soil nails can significantly enhance the shear strength of coral reef slopes, reducing the likelihood of sliding. The arrangement of anchors should be optimized based on the stratified structure and anisotropic properties of reef limestone.

Overall, this paper concludes that the right-side slope of the reef model exhibited good stability under seismic loads with intensities of PGA 0.4 g and below, with no risk of destabilization or damage. For the left-side slope, which was relatively weaker in stability, low-intensity earthquakes (PGA < 0.3 g) had little impact on their stability. However, they showed a moderate risk of destabilization under seismic loads of PGA 0.3 g, and an extremely high risk of destabilization under PGA 0.4 g seismic loading, indicating a very high risk of instability. This demonstrates that the slope showed a significant tendency to destabilize when subjected to earthquakes with intensities of PGA 0.4 g or higher. Potential factors such as slope morphology and external loads significantly affect the stability of coral reef slopes. The differences in the stability of the left and right slopes indicate that the anisotropy of reef limestone and the stratified structure caused by sedimentary characteristics significantly influence the stress distribution and safety factors of the slopes. Dynamic loads have a significant impact on the stability of the reef body, with earthquakes of varying intensities causing a noticeable decrease in the safety factors of both slopes.

5.3. The Impact of Extreme Seismic Conditions on the Stability of Coral Reef Bodies

This study revealed the dynamic response characteristics and stability changes of reef slopes under extreme seismic conditions by introducing actual observed seismic waves into the simulation analysis. The stability of the reef slopes was assessed through a combination of safety factor time-history analysis and permanent displacement analysis.

The application of actual observed seismic waves significantly reduced the safety factor of both side slopes, especially during the peak seismic acceleration period, when the stability of the slopes was at its lowest. Specifically, the lowest factor of safety (FOS) for the left slope was 0.41, indicating that it was close to complete instability under the influence of peak acceleration. This result is linked to its initially low stability, the presence of overlying weak layers, and the potential for the slip surface to expand and deepen during the seismic event, which exacerbates the destabilization tendency. In contrast, the minimum safety factor for the right slope was 2.595, demonstrating strong seismic capacity and remaining well above the critical stability threshold. The strong performance of the right slope can be attributed to the high-strength properties of the framed reef tuff and the significant mitigation of seismic loads due to structural reinforcement.

There is a significant difference in the permanent displacements produced by the left- and right-side slope under extreme seismic conditions. The right-side slope did not experience permanent displacement because the acceleration response values did not exceed the critical acceleration threshold. This result indicates that the right-side slope has strong rigid strength and shear capacity under seismic effects, with negligible risk of sliding. In contrast, the simulation results show that the critical slip surface of the left-side slope experiences a permanent displacement of 2.542 m under seismic loading. This suggests that the left slope has undergone significant slip accumulation due to strong seismic action, and both the depth and extent of the slip may increase, posing a potential threat to the overall stability of the reef.

The actual observed seismic waves had a longer duration and more complex frequency components, which resulted in a more pronounced slope response during the strong seismic interval. Compared to synthetic seismic waves, actual seismic waves provide a more accurate representation of the dynamic instability risk and slip characteristics of slopes under extreme seismic conditions. The artificial wave had a shorter duration (10

s) and a significantly lower peak ground acceleration (PGA). As a result, the permanent displacement of the left slope under the PGA 0.4 g artificial wave condition was much smaller than that under the Kobe wave condition. To more clearly analyze the differences in displacement patterns between the synthetic wave and the Kobe wave, we supplemented the analysis with an artificial wave that had the same PGA as the Kobe wave (PGA 0.83 g) but retained the waveform characteristics of the artificial wave. It can be observed that, due to the similar peak accelerations, the rates of permanent displacement accumulation during the peak acceleration periods were comparable. However, because the Kobe wave had a longer overall duration, a longer peak acceleration duration, and multi-frequency components, the permanent displacement accumulation under the Kobe wave exhibited significant multiple fluctuations. In contrast, under the artificial wave, the permanent displacement accumulation showed rapid growth during the peak acceleration period and almost no accumulation during non-peak dynamic periods.

5.4. Limitations of This Study

Although this study has achieved certain results in the seismic response analysis of coral reef slopes, it still has some limitations, mainly in terms of methodology and assumptions. This study employed the traditional Newmark method for dynamic analysis. While the Newmark method is suitable for dynamic analysis of both linear and nonlinear systems, capable of handling various types of dynamic loads and simulating the dynamic response of complex structures, it has certain limitations [37]. For example, the Newmark method cannot account for the weakening effect of material shear strength under seismic conditions, which may lead to an underestimation of the slope's dynamic response. Additionally, the assumption of a single rigid block behavior in the original Newmark method may result in non-conservative estimates of permanent displacement for shallow sliding masses, thereby affecting the accuracy of slope stability assessment. Discrete element analysis and dynamic response distribution models were also considered in our study. These methods are better suited for capturing the nonlinear behavior of the strata and local stress concentrations. However, due to the high demands for parameter accuracy in these methods, we opted for the more widely applicable Newmark method to avoid potential inaccuracies arising from insufficient parameter precision. Furthermore, the multi-layered coral reef stability analysis model established in this study did not consider the effects of seepage and wave loads. Seepage effects may alter the pore water pressure distribution within the slope, thereby influencing its stability, while wave loads may impose additional dynamic forces on the slope surface. The omission of these factors may lead to overestimation or underestimation of the impact of earthquakes on the stability of coral reef slopes, resulting in some bias in the analysis results. In addition, the range of seismic intensities selected in this study essentially covers the spectrum from light to very strong earthquakes, providing a representative sample for analysis. However, the study did not include seismic conditions with PGAs below 0.05 g (very weak earthquakes) or above 0.4 g (extreme seismic conditions), which represents a limitation in the selection of seismic intensities. To further improve the accuracy and comprehensiveness of the analysis, future research could adopt improved computational methods (e.g., dynamic analysis methods considering material strength weakening effects) and more precise stability evaluation criteria. Moreover, incorporating fluid–structure interaction analysis that considers seepage effects and wave loads will enable a more comprehensive assessment of the stability of multi-layered coral reef slopes, providing a more reliable theoretical basis for practical engineering.

6. Conclusions

This paper focused on the stability of the coral reef body under both natural and seismic conditions, combining static analysis, dynamic response simulation, permanent displacement analysis, and probabilistic stability analysis. It systematically explored the dynamic characteristics and instability risks of the reef body slopes, leading to the following main conclusions:

(1) The static analysis results show that the overall stress distribution of the coral reef body was relatively uniform. The Reef Limestone Slope, with its high shear strength and structural stability, had a safety factor of 19.028. In contrast, the Multi-layered Slope exhibited lower shear strength and a safety factor of 3.314. These findings suggest that under self-weight conditions, the stability of the reef slopes is generally favorable.

(2) Seismic intensity significantly impacted the stability of reef body slopes, with the Multi-layered Slope being more sensitive to seismic loads. Under moderate and strong earthquakes (PGA = 0.3 g and 0.4 g), the minimum factor of safety decreased to 1.09 and 0.804, respectively, resulting in permanent displacements of 1.12 cm and 3.8 cm and estimated instability probabilities of 48% and 100%, respectively.

(3) Under the observed extreme seismic condition, the minimum factor of safety of the Multi-layered Slope decreased to 0.41, with a permanent displacement of 2.542 m, indicating a very high risk of instability. In contrast, the Reef Limestone Slope maintained good stability, attributed to the high-strength properties and reinforcing effects of the framework reef limestone. This highlights the significant impact of slope stratification on seismic performance.

(4) This study analyzed the stability of coral reef slopes under static and seismic conditions. The limitations of the computational methods and model assumptions may lead to overestimating or underestimating the impact of earthquakes on slope stability. Future research incorporating fluid–structure interaction analysis considering seepage effects and wave loads will provide a more comprehensive assessment of multi-layer coral reef slope stability.

Author Contributions: Methodology, investigation, formal analysis, writing—original draft, visualization, R.M.; conceptualization, writing—original draft, review and editing, supervision, B.J.; investigation, visualization, L.Z.; investigation, writing—editing, S.P.; visualization, Writing—editing, K.H. All authors have read and agreed to the published version of the manuscript.

Institutional Review Board Statement: Not applicable.

Informed Consent Statement: Informed consent was obtained from all subjects involved in the study.

Data Availability Statement: Data will be made available on request.

Conflicts of Interest: The authors declare no conflicts of interest.

References

1. Zhu, C.; Liu, H., Zhou, B. Micro-structures and the basic engineering properties of beach calcarenites in South China Sea. *Ocean. Eng.* **2016**, *114*, 224–235. https://doi.org/10.1016/j.oceaneng.2016.01.009.
2. Xu, D.; Zhang, S.; Qin, Y. Study of the micromechanical properties and dissolution characteristics of porous coral reef limestone. *J. Geophys. Res. Solid Earth* **2024**, *129*, e2024JB029131. https://doi.org/10.1029/2024JB029131.

3. Zhu, C.; Qin, Y.; Meng, Q. Formation and sedimentary evolution characteristics of Yongshu Atoll in the South China Sea Islands. *Ocean. Eng.* **2014**, *84*, 61–66. https://doi.org/10.1016/j.oceaneng.2014.03.035.

4. Liu, J.; Cao, L.; Xu, W. Formation and development of coral reefs in the South China Sea. *Palaeogeogr. Palaeoclimatol. Palaeoecol.* **2022**, *594*, 110957. https://doi.org/10.1016/j.palaeo.2022.110957.

5. Zhang, X.; Zhang, L.; Wu, J. Tunnel stability analysis of coral reef limestone stratum in ocean engineering. *Ocean. Eng.* **2022**, *265*, 112636. https://doi.org/10.1016/j.oceaneng.2022.112636.

6. Wu, J.; Fu, H.; Zhang, L. Stability analysis of surrounding rock in underground chamber excavation of coral reef limestone. *Rock Mech. Rock Eng.* **2022**, *55*, 4717–4742. https://doi.org/10.1007/s00603-022-02869-w.

7. Bao, X.; Liu, J.; Li, S. Three-Dimensional Seismic Response Analysis of Zhubi Reef in the South China Sea. *Shock. Vib.* **2021**, *2021*, 2195304. https://doi.org/10.1155/2021/2195304.

8. Bao, X.; Li, S.; Wang, F. Nonlinear seismic response analysis of reef-coral sand site in the South China Sea. *Ocean. Eng.* **2023**, *281*, 114966. https://doi.org/10.1016/j.oceaneng.2023.114966.

9. Zhang, Y.; Ye, J. Seismic dynamics of revetment breakwater built on reclaimed coral sand foundation in the SCS: Insight from 1 g shaking table tests. *Bull. Eng. Geol. Environ.* **2023**, *82*, 134. https://doi.org/10.1007/s10064-023-03172-w.

10. Guo, L.; Zhan, W.; Zhang, F. The influence of earthquakes on Zhubi Reef in the Nansha Islands of the South China Sea. *Acta Oceanol. Sin.* **2017**, *36*, 99–108. https://doi.org/10.1007/s13131-017-1008-0.

11. Tang, Q.; Zhang, J.; Feng, Y. Numerical simulation for shallow strata stability of coral reef in the southwest of Yongshu Reef (South China Sea). *J. Ocean. Univ. China* **2018**, *17*, 763–772. https://doi.org/10.1007/s11802-018-3505-y.

12. Costa, M.B.; Macedo, E.C.; Siegle, E. Wave refraction and reef island stability under rising sea level. *Glob. Planet. Change* **2019**, *172*, 256–267. https://doi.org/10.1016/j.gloplacha.2018.10.015.

13. Wu, Q.; Ding, X.; Zhang, Y. Numerical simulations on seismic response of soil-pile-superstructure in coral sand. *Ocean. Eng.* **2021**, *239*, 109808. https://doi.org/10.1016/j.oceaneng.2021.109808.

14. Wang, X.; Qu, K.; Men, J. Influence of excavation pits on the wave hydrodynamics of fringing reefs under regular waves. *J. Mar. Sci. Eng.* **2023**, *11*, 1464. https://doi.org/10.3390/jmse11071464.

15. Xiao, P.; Liu, H.; Xiao, Y. Liquefaction resistance of bio-cemented calcareous sand. *Soil Dyn. Earthq. Eng.* **2018**, *107*, 9–19. https://doi.org/10.1016/j.soildyn.2018.01.008.

16. Wang, X.; Shan, H.; Wang, X. Strength characteristics of reef limestone for different cementation types. *Geotech. Geol. Eng.* **2020**, *38*, 79–89. https://doi.org/10.1007/s10706-019-01000-1.

17. Luo, Y.; Gong, H.; Wei, X. Dynamic compressive characteristics and damage constitutive model of coral reef limestone with different cementation degrees. *Constr. Build. Mater.* **2023**, *362*, 129783. https://doi.org/10.1016/j.conbuildmat.2022.129783.

18. Zhang, H.; Ren, H.; Mu, C. Experimental study on dynamic mechanical properties and damage characteristics of coral reef limestone. *Constr. Build. Mater.* **2023**, *384*, 131007. https://doi.org/10.1016/j.conbuildmat.2023.131007.

19. Wu, K.; Meng, Q.; Wang, C. Investigation of damage characteristics of coral reef limestone under uniaxial compression based on pore structure. *Eng. Geol.* **2023**, *313*, 106976. https://doi.org/10.1016/j.enggeo.2022.106976.

20. Xu, D.; Zhang, Z.; Qin, Y. Effect of particle size on the failure behavior of cemented coral sand under impact loading. *Soil Dyn. Earthq. Eng.* **2021**, *149*, 106884. https://doi.org/10.1016/j.soildyn.2021.106884.

21. Meng, Q.; Yu, K.; Wang, R. Characteristics of rocky basin structure of Yongshu Reef in the southern South China Sea. *Mar. Georesources Geotechnol.* **2014**, *32*, 307–315. https://doi.org/10.1080/1064119X.2013.764553.

22. Shen, J.; Hu, M.; Wang, X. SWCC of calcareous silty sand under different fines contents and dry densities. *Front. Environ. Sci.* **2021**, *9*, 682907. https://doi.org/10.3389/fenvs.2021.682907.

23. Zhou, J.; Chen, H.; Chen, J. Characteristics and distribution of geohazards since the middle miocene of the Xisha sea area, South China Sea. *Front. Earth Sci.* **2023**, *10*, 1012144. https://doi.org/10.3389/feart.2022.1012144.

24. Wang, X.; Jiao, Y.; Wang, R. Engineering characteristics of the calcareous sand in Nansha Islands, South China Sea. *Eng. Geol.* **2011**, *120*, 40–47. https://doi.org/10.1016/j.enggeo.2011.03.011.

25. Multidisciplinary Oceanographic Expedition Team of Academia Sinica to Nansha Islands (MOETASNI). *Coral Reef Engineering Geology of Nansha Islands*; Science Press: Beijing, China, 1997; pp. 16–61. (In Chinese)

26. Morgenstern, N.R.; Price, V.E. The analysis of the stability of general slip surfaces. *Geotechnique* **1965**, *15*, 79–93. https://doi.org/10.1680/geot.1965.15.1.79.

27. Newmark, N.M. Effects of earthquakes on dams and embankments. *Geotechnique* **1965**, *15*, 139–160.

28. Jibson, R.W.; Harp, E.L.; Michael, J.A. A method for producing digital probabilistic seismic landslide hazard maps. *Eng. Geol.* **2000**, *58*, 271–289. https://doi.org/10.1016/S0013-7952(00)00039-9.

29. Duncan, J.; Wright, S.; Brandon, T. *Soil Strength and Slope Stability*; John Wiley & Sons: Hoboken, NJ, USA, 2014.

30. Landslide, P.E.I. Sliding Block Analysis. *Transp. Res. Rec.* **1993**, *1411*, 9–17.

31. GeoStudio International Ltd. *GeoStudio User's Manual*; GeoStudio International Ltd.: Calgary, AB, Canada, 2023.

32. Wood, H.; Neumann, F. The Modified Mercalli Intensity Scale of 1931. *Bull. Seismol. Soc. Am.* **1931**, *21*, 277–283. https://doi.org/10.1785/BSSA0210040277.

33. Liu, H.; Kang, F.; Gao, Y. Time history analysis method of slope seismic stability (in Chinese). *Rock Soil Mech.* **2003**, *24*, 553–556.

34. Griffiths, D.; Lane, P. Slope stability analysis by finite elements. *Geotech. Lond.* **2001**, *51*, 653–654.

35. Jibson, R.W.; Michael, J.A. *Maps Showing Seismic Landslide Hazards in Anchorage, Alaska*; US Geological Survey: Reston, VA, USA, 2009.

36. Bray, J.; Rodriguez-Marek, A. Characterization of forward-directivity ground motions in the near-fault region. *Soil Dyn. Earthq. Eng.* **2004**, *24*, 815–828. https://doi.org/10.1016/j.soildyn.2004.05.001.

37. Song, J.; Feng, Q.; Chen, T.A. multi-block sliding approach to calculate the permanent seismic displacement of slopes. *Eng. Geol.* **2019**, *255*, 48–58.